

Chapter 1

Introduction

1.1 Brief History and Introduction

Electric cars have been created in response to the shortcomings of the common internal combustion engine (ICE). They have several benefits, including cheaper running costs, lower pollution, and quieter operation. Battery electric cars (BEVs), plug-in hybrid electric vehicles (PHEVs), and hybrid electric vehicles (HEVs) are just a few examples of the several types of EVs available. In the early nineteenth century, people started thinking about electric automobiles. Robert Anderson and Thomas Davenport were two inventors who first investigated electric propulsion in the 1830s. They created the first electric vehicles that used primary batteries that could not be recharged. The use of electric cars saw an enormous increase in the late 19th and early 20th centuries. When compared to early gasoline-powered cars, they were preferred due to their convenience and cleanliness. For short trips around town or as taxis, electric vehicles were widely used. Improvements to the internal combustion engine were another 20th-century phenomenon that lowered the entry price of gasoline-powered automobiles. Because of issues with range, charging infrastructure, and the introduction of fossil fuel infrastructure, electric vehicles steadily lost attraction. The last decades of the 20th century experienced an increase in interest in electric vehicles as a solution to pollution and oil dependence issues. To combat climate change and to promote environmentally friendly transportation, governments and organizations have begun funding electric car research and development. The market for electric vehicles experienced an enor-

mous shift in the 21st century. The development of lithium-ion batteries, improvements in the efficiency of electric motors, and the spread of charging stations have all contributed to the widespread availability of modern electric vehicles. Successful electric vehicle models introduced by companies like Tesla, Nissan, and Chevrolet increased public acceptance and market expansion. Policies and incentives have been put in place by governments all over the world to promote the growing popularity of electric vehicles. Increased financial support, tax benefits, and limited emission rules have all contributed to the rapid expansion of the electric vehicle market. Technology improvements, falling prices, and the push towards greener transportation options are projected to support the EV industry's continued expansion.

Higher conversion efficiencies, higher power densities, and superior low-speed torque characteristics are just a few of the ways in which electric motors beat internal combustion engines. During deceleration or braking, an electric vehicle's regenerative braking system converts the kinetic energy of the vehicle's moving parts into electrical energy using the electric motor as a generator. This function aids in battery recharging and improves overall energy efficiency.

1.2 Significance of Induction Motor

When compared to Induction Motors (IM), Synchronous Motors have better efficiency [1], better power-to-weight ratio, higher torque density, and capability to operate at unity or leading power factor. Induction motors are known for their robust construction and ability to withstand harsh operating conditions. They are simpler than synchronous motors and do not require permanent magnets, so they last longer and are less likely to lose their magnetism. When compared to synchronous motors, induction motors provide lower costs of manufacture because of their simpler design, which does not require permanent magnets. The squirrel cage rotor used in induction motors provides built-in resistance to failure. The motor continues to run at a lower level of efficiency if the rotor bars are broken or there is a short circuit. Any damage to the rotor of a synchronous motor might cause the motor to stop working.

1.3 Control of Induction Motor

V/F Control of the IM, which is a scalar control method, has good steady-state response but poor transient response. Whereas in vector control, both steady state and transient responses are improved. The vector control method is implemented in a synchronously rotating reference frame [2]. Hence the rotor flux angle is required to transform the variables from synchronously rotating reference frame to abc frame for actual motor control.

Two methods are employed for measuring rotor flux angle. Measurement of rotor flux using sensors is known as direct vector control, but it is a less accurate method. The Indirect Vector control method is often used; the accuracy of this method depends on the accuracy with which the rotor time constant is estimated. Rotor resistance changes with motor loading due to change in temperature. So online rotor resistance estimation is required. Maximum torque per ampere control of the induction motor is chosen to achieve a reduction in energy consumption. The MTPA control method generates the required torque while consuming as little stator current as feasible.

1.4 Objectives of the Thesis

Implementation of rated-flux indirect vector control and MTPA control for induction motor control is the focus of this thesis. There is also a comparison of the outcomes. Hardware implementation of both the control schemes is attempted.

More specifically, the study aims at:

- Modeling of induction motor in Synchronous Reference Frame.
- Development of the control method for the Indirect Vector (IV) control scheme.
- Development of the control method for the Maximum Torque Per Ampere (MTPA) control scheme.
- Hardware Implementation of IV control and MTPA control methods using TMS320F28335 microcontroller and comparison of the results.

1.5 Organization of the Thesis

The thesis is divided into six chapters, each of which is described briefly below:

- **Chapter-1:** This chapter provides a history of electric vehicles. It also discusses the significance and control of induction motors.
- **Chapter-2:** This chapter explains the modeling of induction motor in synchronous rotating reference frame. Indirect Vector control technique is discussed in detail. Simulation results are shown.
- **Chapter-3:** This chapter comes up with Maximum torque per ampere control scheme, where maximum torque can be achieved at minimum current. Expressions are derived for rotor flux which is sensitive to the load.
- **Chapter-4:** This chapter discusses the experimental implementation using the TI's TMS320F28335 microcontroller. Hardware results are presented for both indirect vector control and MTPA control methods. It is shown that MTPA control method draws lesser current at a given load.
- **Chapter-5:** In this chapter, conclusions and scope for the future work are discussed

Chapter 2

Indirect Vector Control of Induction Motor

2.1 Modeling of Induction Motor

Modeling of an induction machine can be done in two ways.

- Modeling in actual phase variables.
- Modeling in d-q references frame.

Some advantages can be gained by changing variables from abc to dq0. The primary motivation for making the transformation from the 3-phase instantaneous voltages and currents frame to the dq0 references frame is to enable a simpler execution of numerical calculations. In addition, DC (constant) values may be controlled efficiently and robustly with the use of feedback controllers like PI and PID. However, the integrator term (i.e., $1/s$) of these feedback controllers often does not provide an infinite gain when the input values are periodic or sinusoidal. As a result, the steady-state error is not be eliminated. By transforming the variables from abc to dq0, a complex model may be reduced to a simple dynamic model. This leads to ease of analysis and computation of the system model.

2.2 Reference Frame Theory

Three types of reference frames used are:

- Stationary reference frame (or $\alpha\beta$ reference frame)
- Rotor reference frame (or xy reference frame)
- Synchronously rotating reference frame (or dq reference frame)

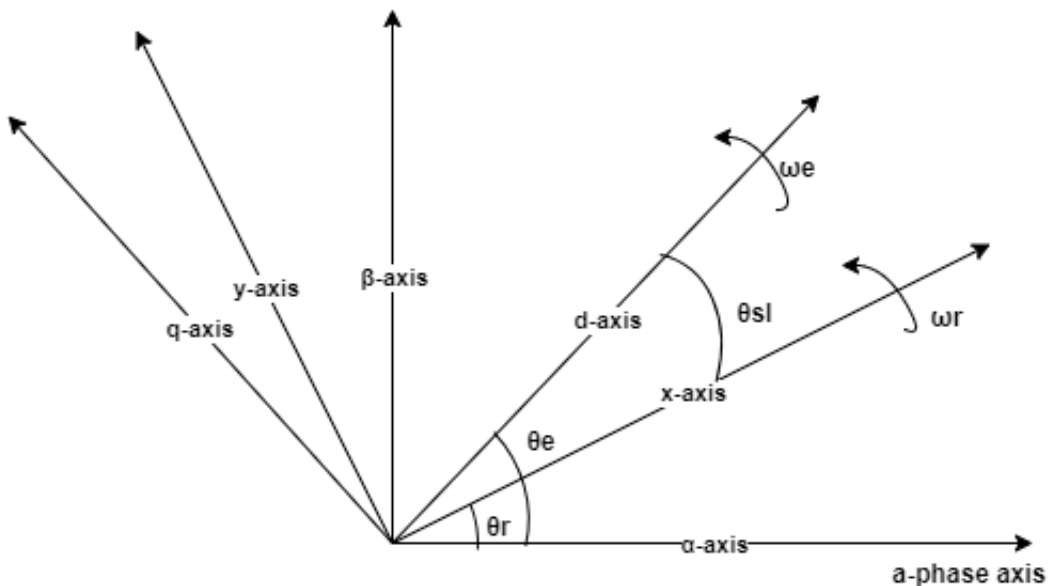


Figure 2.1: Reference Frames

In Figure 2.1, it is seen that $\alpha\beta$, x-y, d-q axes are orthogonal to each other respectively. x-axis is aligned at θ_r angle with stationary a-phase axis and is rotating at rotor speed ω_r . d-axis is aligned at θ_e angle with stationary a-phase axis and is rotating at synchronous speed ω_e .

Transformation from abc to dqr is given as

$$i_d = \frac{2}{3}[i_a \cos(\theta) + i_b \cos(\theta_1) + i_c \cos(\theta_2)] \quad (2.1)$$

$$i_q = \frac{2}{3}[-i_a \sin(\theta) - i_b \sin(\theta_1) - i_c \sin(\theta_2)] \quad (2.2)$$

$$i_0 = \frac{1}{3}(i_a + i_b + i_c) \quad (2.3)$$

where $\theta = \omega t$, $\theta_1 = \theta - \frac{2\pi}{3}$, $\theta_2 = \theta + \frac{2\pi}{3}$.

Hence, the transformation matrix from abc to dqr is

$$C_s = \frac{2}{3} \begin{bmatrix} \cos(\theta) & \cos(\theta_1) & \cos(\theta_2) \\ -\sin(\theta) & -\sin(\theta_1) & -\sin(\theta_2) \\ \frac{1}{2} & \frac{1}{2} & \frac{1}{2} \end{bmatrix} \quad (2.4)$$

Let the speed of the reference frame be ω .

If $\omega = 0$, the reference frame is called stationary or $\alpha\beta$ -reference frame, i.e., $\theta = 0$.

If $\omega = \omega_r$, the reference frame is called rotor reference frame, i.e., $\theta = \theta r$.

If $\omega = \omega_e$, the reference frame is called synchronously rotating reference frame, i.e., $\theta = \theta e$.

If $\omega = \text{arbitrary}$, the reference frame is called arbitrarily rotating reference frame, i.e., $\theta = \theta$.

2.3 Modeling of IM in Synchronous Reference Frame

The synchronous reference frame is used for the IM model. The dynamic equations of an induction motor in synchronous reference frame can be written as,

$$v_{ds}^e = r_s i_{ds}^e + \frac{d}{dt} \psi_{ds}^e - \omega_e \psi_{qs}^e \quad (2.5)$$

$$v_{qs}^e = r_s i_{qs}^e + \frac{d}{dt} \psi_{qs}^e + \omega_e \psi_{ds}^e \quad (2.6)$$

$$v_{dr}^e = r_r i_{dr}^e + \frac{d}{dt} \psi_{dr}^e - (\omega_e - \omega_r) \psi_{qr}^e \quad (2.7)$$

$$v_{qr}^e = r_r i_{qr}^e + \frac{d}{dt} \psi_{qr}^e + (\omega_e - \omega_r) \psi_{dr}^e \quad (2.8)$$

$$\psi_{ds}^e = l_s i_{ds}^e + l_m i_{dr}^e \quad (2.9)$$

$$\psi_{qs}^e = l_s i_{qs}^e + l_m i_{qr}^e \quad (2.10)$$

$$\psi_{dr}^e = l_r i_{dr}^e + l_m i_{ds}^e \quad (2.11)$$

$$\psi_{qr}^e = l_r i_{qr}^e + l_m i_{qs}^e \quad (2.12)$$

The following matrix equation is obtained by substituting the expression for fluxes in (2.9), (2.10), (2.11) and (2.12) into (2.5), (2.6), (2.7), and (2.9).

$$\begin{bmatrix} v_{ds}^e \\ v_{qs}^e \\ v_{dr}^e \\ v_{qr}^e \end{bmatrix} = \begin{bmatrix} r_s + l_s p & -\omega_e l_s & l_m p & -\omega_e l_m \\ \omega_e l_s & r_s + l_s p & \omega_e l_m & l_m p \\ l_m p & -(\omega_e - \omega_r) l_m & r_r + l_r p & -(\omega_e - \omega_r) l_r \\ (\omega_e - \omega_r) l_m & l_m p & (\omega_e - \omega_r) l_r & r_r + l_r p \end{bmatrix} \begin{bmatrix} i_{ds}^e \\ i_{qs}^e \\ i_{dr}^e \\ i_{qr}^e \end{bmatrix} \quad (2.13)$$

(2.13)

$$(\because \frac{d}{dt} = p)$$

$$\begin{aligned} &= \begin{bmatrix} r_s & 0 & 0 & 0 \\ 0 & r_s & 0 & 0 \\ 0 & 0 & r_r & 0 \\ 0 & 0 & 0 & r_r \end{bmatrix} \begin{bmatrix} i_{ds}^e \\ i_{qs}^e \\ i_{dr}^e \\ i_{qr}^e \end{bmatrix} + \begin{bmatrix} l_s & 0 & l_m & 0 \\ 0 & l_s & 0 & l_m \\ l_m & 0 & l_r & 0 \\ 0 & l_m & 0 & l_r \end{bmatrix} p \begin{bmatrix} i_{ds}^e \\ i_{qs}^e \\ i_{dr}^e \\ i_{qr}^e \end{bmatrix} + \omega_e \begin{bmatrix} 0 & -l_s & 0 & -l_m \\ l_s & 0 & l_m & 0 \\ 0 & 0 & 0 & 0 \\ 0 & 0 & 0 & 0 \end{bmatrix} \begin{bmatrix} i_{ds}^e \\ i_{qs}^e \\ i_{dr}^e \\ i_{qr}^e \end{bmatrix} \\ &\quad + (\omega_e - \omega_r) \begin{bmatrix} 0 & 0 & 0 & 0 \\ 0 & 0 & 0 & 0 \\ 0 & -l_m & 0 & -l_r \\ l_m & 0 & l_r & 0 \end{bmatrix} \begin{bmatrix} i_{ds}^e \\ i_{qs}^e \\ i_{dr}^e \\ i_{qr}^e \end{bmatrix} \end{aligned} \quad (2.14)$$

$$[\bar{V}] = [R][\bar{I}] + [L]p[\bar{I}] + \omega_e[G1][\bar{I}] + (\omega_e - \omega_r)[G2][\bar{I}] \quad (2.15)$$

$$p[\bar{I}] = [L]^{-1}[[\bar{V}] - [R][\bar{I}] - \omega_e[G1][\bar{I}] - (\omega_e - \omega_r)[G2][\bar{I}]] \quad (2.16)$$

Air gap power is $\bar{I}^T [G2] \omega_r \bar{I}$ which appears when we premultiply (??) with \bar{I}^T

$$T_e \times \omega_{rm} = P_{ag} = \bar{I}^T [G2] \bar{I} \times \omega_r \quad (2.17)$$

Where ω_{rm} is rotor mechanical speed in rad/sec and T_e is electromagnetic torque.

$$T_e = \frac{P}{2} \bar{I}^T [G2] \bar{I} \quad (2.18)$$

$$T_e = \frac{3P}{2} l_m (i_{dr}^e i_{qs}^e - i_{qr}^e i_{ds}^e) \quad (2.19)$$

$$\begin{aligned}
 &= \frac{J}{(\frac{P}{2})} \frac{d\omega_r}{dt} + \frac{B}{(\frac{P}{2})} + T_L \\
 \frac{d\omega_r}{dt} &= \frac{P}{2J} (T_e - T_L - \frac{2B}{P} \omega_r)
 \end{aligned} \tag{2.20}$$

Using (2.16), (2.19) and (2.20) modeling of induction motor can be done.

2.4 Indirect Vector Control

2.4.1 Field Orientated Control or Vector Control of IM

Control method is referred to as field-oriented control due to the fact that control is executed in field coordinates. It is also referred to as vector control since it is related to phasor control of flux linkages.

Vector control schemes can be classified as:

- Rotor flux-oriented vector control (RFOC)
- Air gap flux-oriented vector control (AFOC)
- Stator flux oriented vector control (SFOC)

Motivation for RFOC:

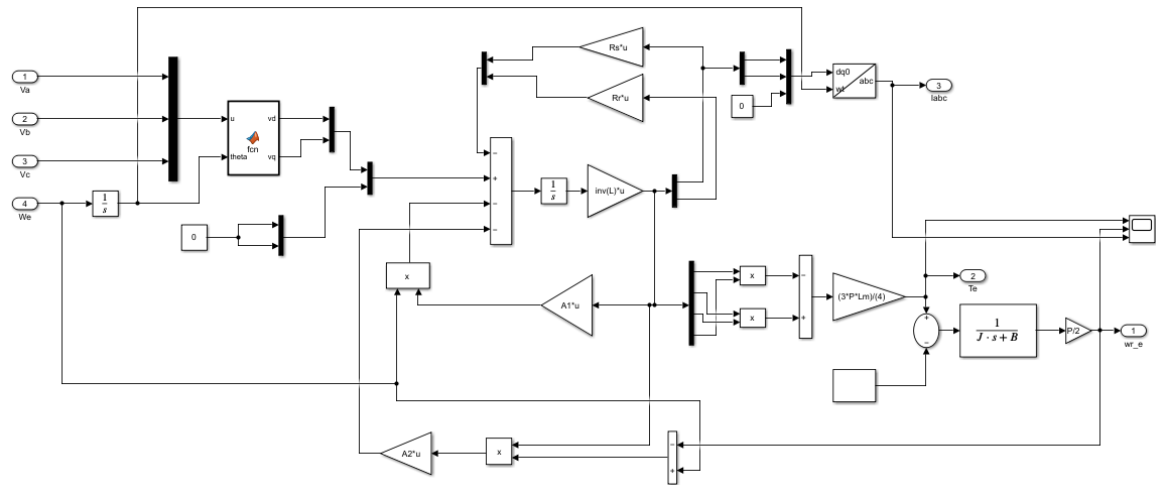
Rotor flux oriented vector control has inherent decoupling between the rotor flux and the stator torque component of current. In AFOC, airgap flux is more easily accessible than in RFOC. However, AFOC is not inherently decoupled control of flux and torque. Hence extra decoupling circuit is required for this control.

In SFOC, stator flux is more easily accessible than in RFOC and AFOC.

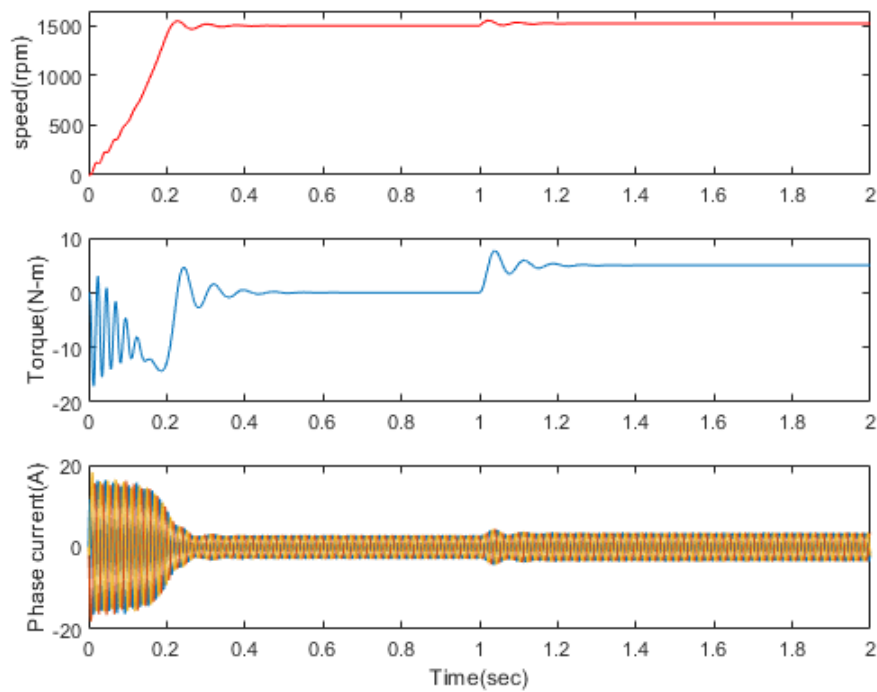
i_{ds} = Flux component of current

i_{qs} = Torque component of current

Flux in the stator is dependent on not just i_{ds} but also on i_{qs} and w_{sl} . Since i_{qs} affects both the stator flux and the generated torque, it is difficult to adjust each variable independently. w_{sl} is also dependent on both components of the stator current. Because of this, both feedback and feed-forward SFOC method require a more complicated calculation of angular slip speed to estimate the stator flux position.



(a) Simulink Model of IM



(b) IM is supplied with 230V rms, 50 hz frequency. Load Torque = 5 N-m is given at t = 1sec

Figure 2.2: IM model and simulation results

2.4.2 Rotor Flux Orientated Vector Control

Decoupling [3] and individually managing the magnetizing flux and torque-producing current components allows for accurate control of an induction motor (IM) using Rotor Flux Oriented control. Torque and flux may be adjusted individually, much as in a separately excited DC motor. Rotor flux in the DC motor is aligned statically (i.e, rotor flux in DC machine is stationary) whereas in the induction motor, rotor flux is synchronously rotating. So, the position of rotor flux is estimated at every instance. With this said, if the rotor flux angle is estimated correctly, then the induction motor's control can be seen like the DC motor. This vector control is called Rotor flux-orientated vector control. There are two distinct varieties of vector control, distinguished by the means by which the rotor flux position is measured. They are

- Direct Vector Control
- Indirect Vector Control

2.4.2.1 Direct Vector Control

Direct vector control is used when the rotor flux position is measured by terminal voltages and currents, flux measuring coils, or hall effect sensors. The flux is estimated by integration of induced emf at higher speeds. At lower speeds, the flux estimation is inaccurate due to reduced induced emf and associated error in integration. Often current based flux estimation is preferred at low speed (less than 10% of rated speed).

2.4.2.2 Indirect Vector Control

Indirect Vector control is used when the position of the flux is inferred using the rotational speed of the motor and motor parameters. Since the flux location is approximated using the motor's parameters, this approach is sensitive to changes in IM parameters, specifically the rotor and stator time constant. The time constant of the rotor has an effect on the flux positions estimator used in indirect rotor flux oriented control [4]. The stator time constant is particularly important in the regulation of stator flux-oriented vectors in stator. Stator and rotor time constant have a role in air gap flux-oriented control.

Therefore, indirect rotor flux oriented vector control necessitates rotor time constant estimate. Variations in rotor resistance caused by the temperature effect are also important.

Advantages of Indirect Vector control

- Indirect vector control shows substantial improvement over direct vector control in terms of dynamic performance.
- In contrast to direct vector control, drift is not an issue here.
- Elimination of hall effect sensors reduces the overall installation cost.

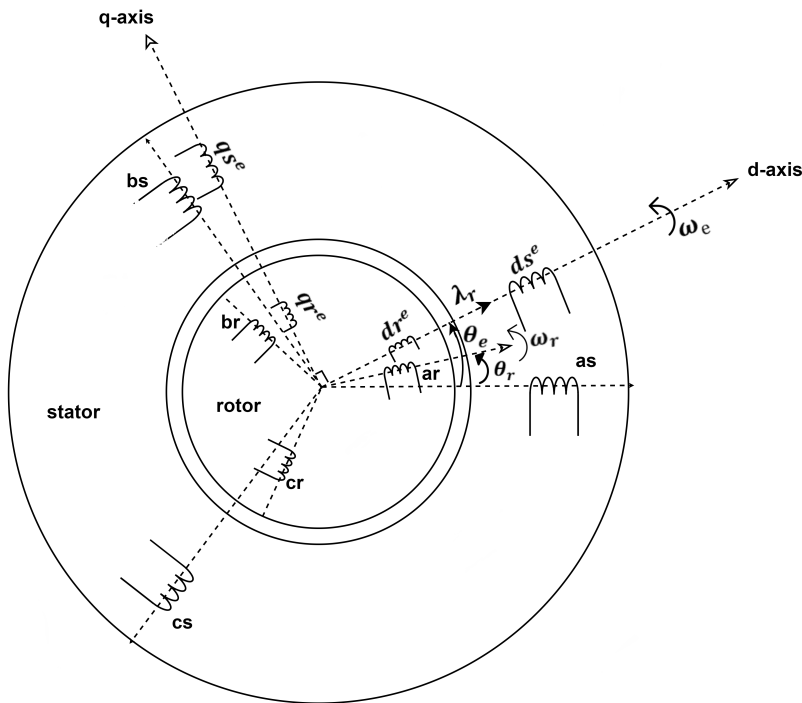


Figure 2.3: Rotor flux oriented IM

The superscript 'e' represents the rotor flux reference frame. Three stationary a,b, and c axes are displaced with a 120-degree angle. Two rotating vectors are present. One is a synchronously rotating vector at ω_e and making angle of θ_e with respect to stationary phase 'a' axis. Another is aligned with the rotor frame which rotates at ω_r and makes an angle of θ_r with respect to the stationary phase 'a' axis. Rotor flux is aligned with the d-axis of the synchronous rotating vector. It is feasible to implement rotor flux-oriented control if

the motor equations are derived in rotor flux reference frame where d-axis is aligned along the rotor flux vector.

From the Figure 2.3, we can write the motor equations as follows.

$$v_{ds}^e = r_s i_{ds}^e + \frac{d}{dt} \psi_{ds}^e - \omega_e \psi_{qs}^e \quad (2.21)$$

$$v_{qs}^e = r_s i_{qs}^e + \frac{d}{dt} \psi_{qs}^e + \omega_e \psi_{ds}^e \quad (2.22)$$

$$v_{dr}^e = r_r i_{dr}^e + \frac{d}{dt} \psi_{dr}^e - (\omega_e - \omega_r) \psi_{qr}^e \quad (2.23)$$

$$v_{qr}^e = r_r i_{qr}^e + \frac{d}{dt} \psi_{qr}^e + (\omega_e - \omega_r) \psi_{dr}^e \quad (2.24)$$

$$\psi_{ds}^e = l_s i_{ds}^e + l_m i_{dr}^e \quad (2.25)$$

$$\psi_{qs}^e = l_s i_{qs}^e + l_m i_{qr}^e \quad (2.26)$$

$$\psi_{dr}^e = l_r i_{dr}^e + l_m i_{ds}^e \quad (2.27)$$

$$\psi_{qr}^e = l_r i_{qr}^e + l_m i_{qs}^e \quad (2.28)$$

Figures 2.4 and 2.5 depict the dq equivalent circuits of an IM in synchronous reference frame.

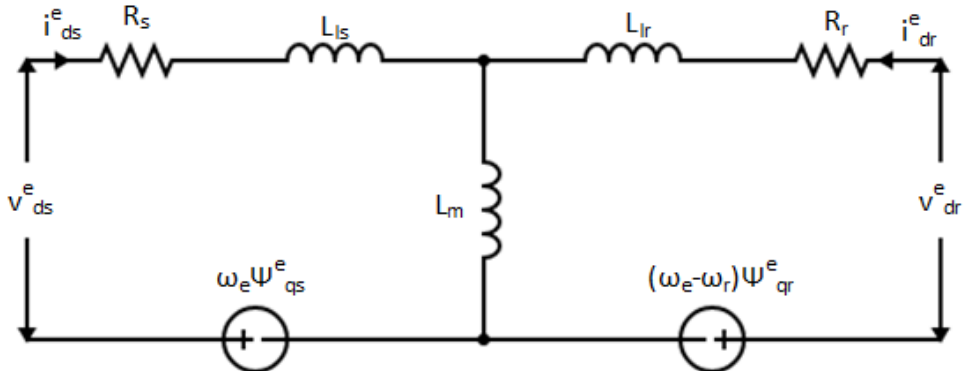


Figure 2.4: Equivalent circuit of IM along d-axis

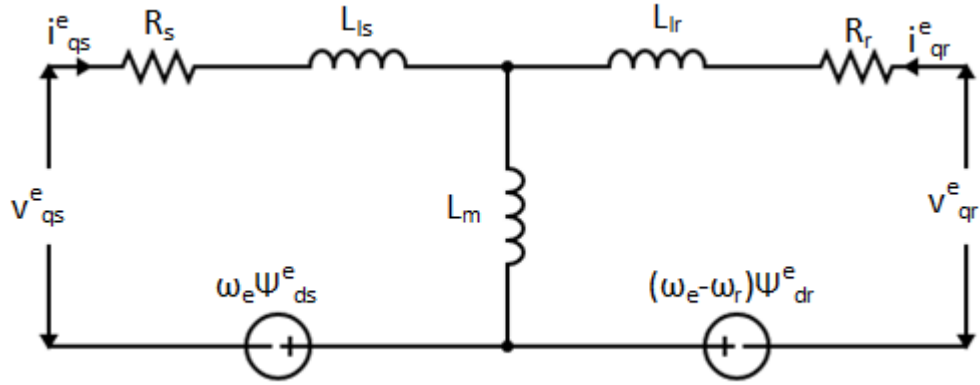


Figure 2.5: Equivalent circuit of IM along q-axis

The d-axis is aligned with rotor flux. As a result, the component of the rotor flux vector along the q-axis is zero, while the component along the d-axis is equal to the rotor flux.

$$\psi_{dr}^e = \psi_r \quad (2.29)$$

$$\psi_{qr}^e = 0 \quad (2.30)$$

$$\psi_{dr}^e = \text{constant} \quad (2.31)$$

As the rotor bars are shorted, from (2.23) and (2.24), the following equations can be written

$$0 = R_r i_{dr}^e + \frac{d}{dt} \psi_{dr}^e - (\omega_e - \omega_r) \psi_{qr}^e \quad (2.32)$$

$$0 = R_r i_{qr}^e + \frac{d}{dt} \psi_{qr}^e + (\omega_e - \omega_r) \psi_{dr}^e \quad (2.33)$$

Substituting ψ_{dr}^e and ψ_{qr}^e from (2.29), (2.30) and (2.31) in (2.32), the following equation is obtained

$$i_{dr}^e = 0 \text{ which means } dr \text{ winding is absent} \quad (2.34)$$

(2.25) becomes

$$\psi_{dr}^e = l_m i_{ds}^e \quad (2.35)$$

From (2.28) and (2.30),

$$i_{qr}^e = -\left(\frac{l_m}{l_r}\right) i_{qs}^e \quad (2.36)$$

Substituting (2.26) and (2.30) into (2.33) gives

$$(\omega_e - \omega_r) = \omega_{sl} = \frac{R_r}{l_r} \frac{l_m i_{qs}^e}{\psi_{dr}^e} \quad (2.37)$$

From (2.35),

$$\omega_{sl} = \frac{1}{\tau_r} \frac{i_{qs}^e}{i_{ds}^e} \quad (2.38)$$

where $\tau_r = \frac{l_r}{r_r}$, which is rotor time constant.

Electromagnetic torque equation is given as

$$T_e = \frac{3P}{2} \frac{l_m}{2} (i_{dr}^e i_{qs}^e - i_{qr}^e i_{ds}^e) \quad (2.39)$$

Substituting (2.34) and (2.36) into (2.39), the electromagnetic torque equation can be written as

$$T_e = \frac{3P}{2} \frac{l_m^2}{2} \frac{i_{ds}^e i_{qs}^e}{l_r} \quad (2.40)$$

For vector transform, we need slip speed

From the Figure 2.3

$$\theta_e = \int \omega_e dt = \int (\omega_{sl} + \omega_r) dt \quad (2.41)$$

Classification Based on Inverter Control Techniques

- Current Controlled Voltage Source Inverter (CCVSI)
- Voltage Controlled Voltage Source Inverter (VCVSI)

2.5 Current Controlled Voltage Source Inverter (CCVSI)

Actual current follows reference current within the hysteresis band which is shown in Figure 2.6. The block diagram in Figure 2.7 shows the implementation of Indirect Vector control with Current Controlled VSI. Here, i_{as} , i_{bs} and i_{cs} are the measured phase currents from the motor terminals. Whereas i_{as}^* , i_{bs}^* and i_{cs}^* represent the reference currents. Measured and reference currents are fed to the hysteresis current controller.

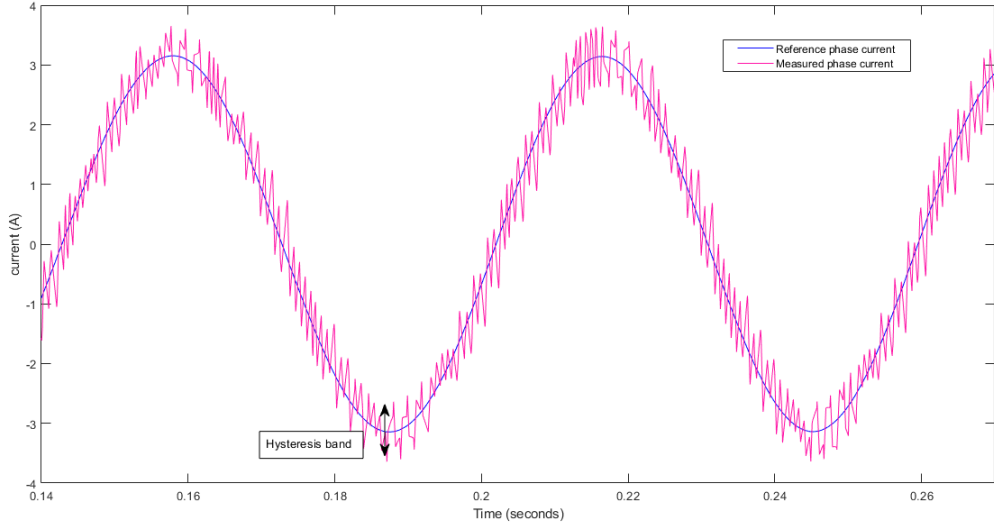


Figure 2.6: Hysteresis current control

The algorithm for the HCC is as follows:

$$h = \text{hysteresis band}$$

If $(i_{as}^* - i_{as}) \geq h$ then upper switch of inverter ON,
lower switch of inverter OFF.

If $(i_{as}^* - i_{as}) \leq -h$ then upper switch of inverter OFF,
lower switch of inverter ON.

In Indirect Vector control, the reference rated rotor flux linkage (ψ_r^*) must be calculated for knowing the reference current i_{ds}^{e*} [5].

The motor parameters are given in Appendix A.

Star connected stator, $V_{l-lrms} = 415V(\text{rated})$, $f_{\text{rated}} = 50Hz$

$$V_{ph-\text{peak}} = \frac{415 \times \sqrt{2}}{\sqrt{3}} = \omega_e \times \psi_s \simeq \omega_e \times \psi_r$$

$$\psi_r^* = \frac{\frac{415 \times \sqrt{2}}{\sqrt{3}}}{2 \times \pi \times 50} = 1.07899 \text{ wb-turns}$$

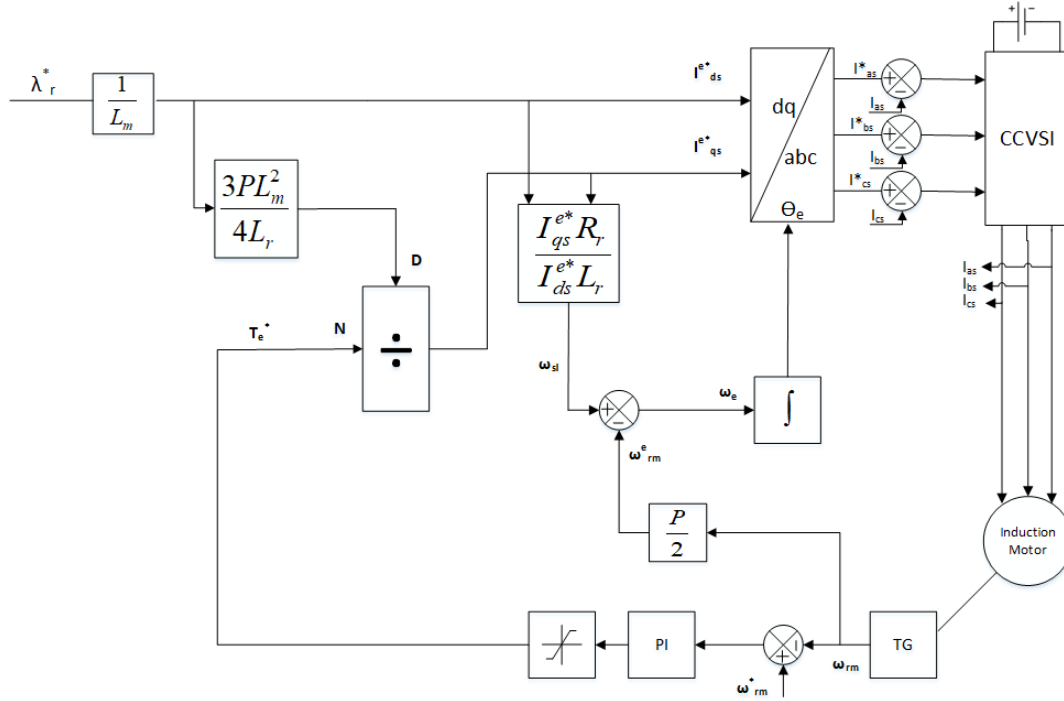


Figure 2.7: Block diagram of Indirect Rotor-Flux Oriented Vector Controlled IM drive fed from a current regulated pulse width modulated VSI

Hysteresis current controller(HCC) with a VSI has the disadvantage of the variable switching frequency. Switching frequency is not constant and depends on various parameters like DC link Voltage and motor parameters. And switching frequency is not known. This issue can be addressed by Voltage based control method.

2.6 Voltage Controlled Voltage Source Inverter (VCVSI)

Stator Voltages are to be computed to supply the motor voltage equations in synchronously rotating reference frame.

Substituting (2.25) and (2.26) into (2.21) and (2.22) gives

$$v_{ds}^e = r_s i_{ds}^e + \frac{d}{dt}(l_s i_{ds}^e + l_m i_{dr}^e) - \omega_e(l_s i_{qs}^e + l_m i_{qr}^e) \quad (2.42)$$

$$v_{qs}^e = r_s i_{qs}^e + \frac{d}{dt}(l_s i_{qs}^e + l_m i_{qr}^e) + \omega_e(l_s i_{ds}^e + l_m i_{dr}^e) \quad (2.43)$$

from (2.27)

$$i_{dr}^e = \left(\frac{\psi_{dr}^e - l_m i_{ds}}{l_r} \right) \quad (2.44)$$

from (2.28)

$$i_{qr}^e = \left(\frac{\psi_{qr}^e - l_m i_{qs}}{l_r} \right) = \left(\frac{-l_m i_{qs}}{l_r} \right) \therefore \psi_{qr}^e = 0 \quad (2.45)$$

Note: $\sigma = (1 - \frac{l_m^2}{l_s l_r})$ denotes leakage factor of the induction motor.

Eliminating rotor currents using (2.44) and (2.45) in (2.42) and (2.43)

$$v_{ds}^e = \underbrace{r_s i_{ds}^e + \sigma l_s \frac{d}{dt} i_{ds}^e}_{v_{ds}^{e'}} + \underbrace{\frac{l_m}{l_r} \frac{d}{dt} \psi_{dr}^e - \omega_e \sigma l_s i_{qs}^e}_{v_{ds-dd}^e} \quad (2.46)$$

$$v_{qs}^e = \underbrace{r_s i_{qs}^e + \sigma l_s \frac{d}{dt} i_{qs}^e}_{v_{qs}^{e'}} + \underbrace{\omega_e \frac{l_m}{l_r} \psi_{dr}^e + \omega_e \sigma l_s i_{ds}^e}_{v_{qs-dd}^e} \quad (2.47)$$

The implementation of indirect vector control with voltage controlled VSI is represented in Figure 2.8 block diagram.

According to the speed of the motor, the tacho generator will generate voltage accordingly. And this measured speed is compared with the reference speed. The speed error signal is then passed to the speed loop PI controller k_p, k_i are well designed for getting reference torque from the speed error signal.

With the help of reference torque and rated rotor flux, reference dq axes currents are produced. Phase currents from the motor are sensed and transformed to dq reference axes (as discussed in section 2.2) and then compared with reference dq axes which are then passed to the current loop PI controller. k_p, k_i are well designed and tuned for getting reference voltage. This voltage is transformed back to abc axes and PWM pulses are generated which are then feed to the gate drive circuit of the VSI. By this means, the switching frequency can be kept at the desired value.

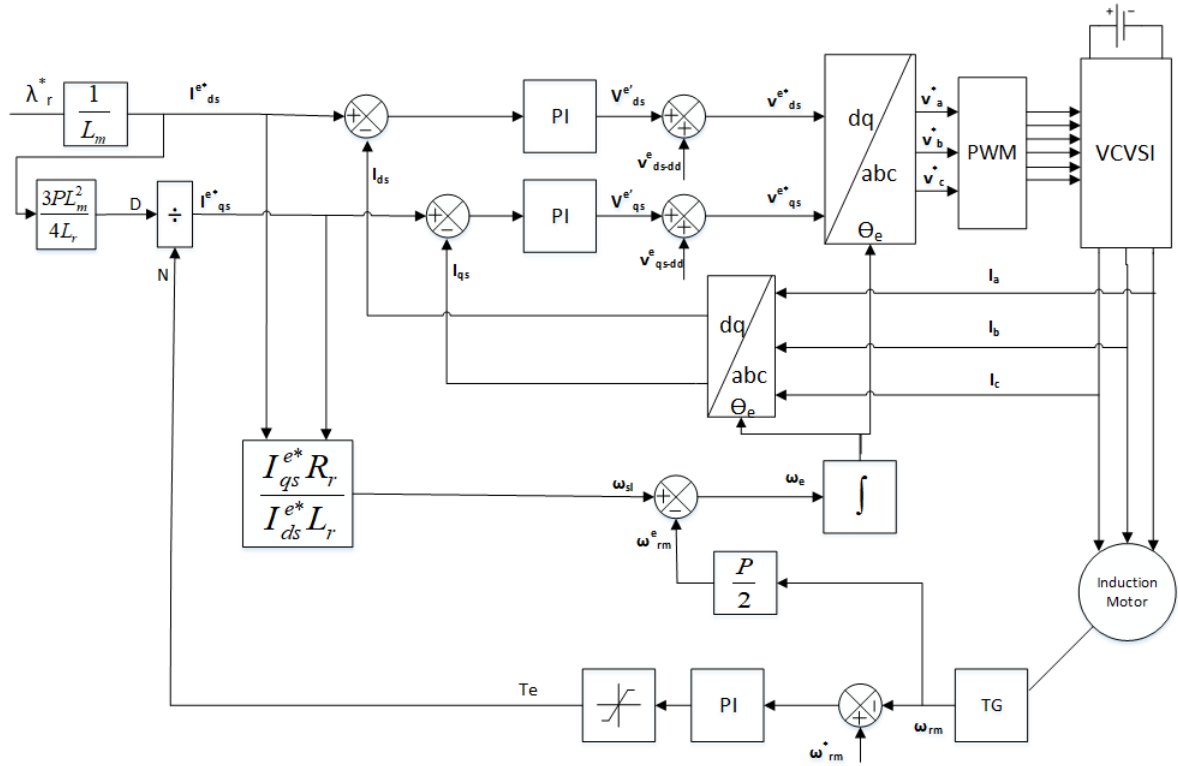


Figure 2.8: Block diagram of Rated-flux Indirect Vector control using VCVSI

Estimation of Rotor Resistance of IM

For vector transform, slip speed estimation is crucial which is the function of time constant of the rotor. Variation of rotor inductance is more in saturation and field weakening operations which are not a concern as the rotor flux is kept constant. So, variation in rotor resistance must be captured online because no test like blocked rotor, no load, and DC resistance test can give real-time rotor resistance. Plenty of methodologies are available in the literature [6–17]. A few disadvantages are (i) it is slow and sensitive to load changes, (ii) it requires complex mathematical computation. Using the dynamic model of the induction motor in two reference frames, this thesis proposes a method for accurately estimating the resistance of the rotors. To account for temperature change, there is a more practical method of calculating the rotor resistance that just uses the stator temperatures. Neither of these approaches requires complex calculations or extensive hardware changes. Therefore, they have been validated for use in automotive applications.

2.7 Simulation Results

Figure 2.9 shows torque, speed, and phase currents. At $t=0$ sec, the reference speed is 500 rpm and the reference torque is 1 N-m. Load torque of 3.5 N-m is given in a step change at $t=2$ sec with reference speed = 1300 rpm. Transient and steady-state response can be observed. Figure 2.10 depicts the rotor flux. The d-axis rotor flux is made equal to the total rotor flux in the indirect vector control method which is constant and the q-axis rotor flux is made zero. Figure 2.11 depicts i_{ds}^e and i_{qs}^e components of current. i_{ds}^e is constant because it is flux component of current and i_{qs}^e is the torque component of current and it is sensitive to load changes.

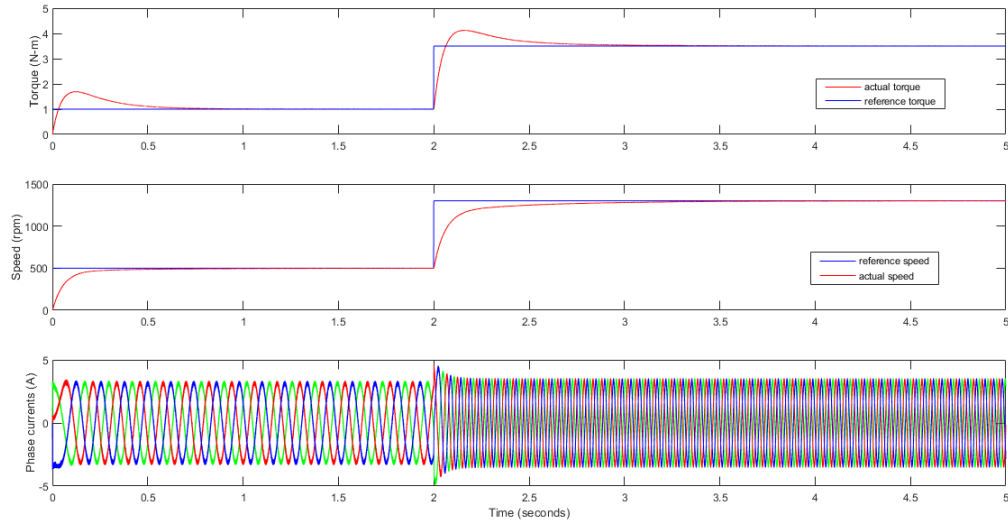


Figure 2.9: Torque, Speed, Phase currents plots are shown for Indirect Vector control

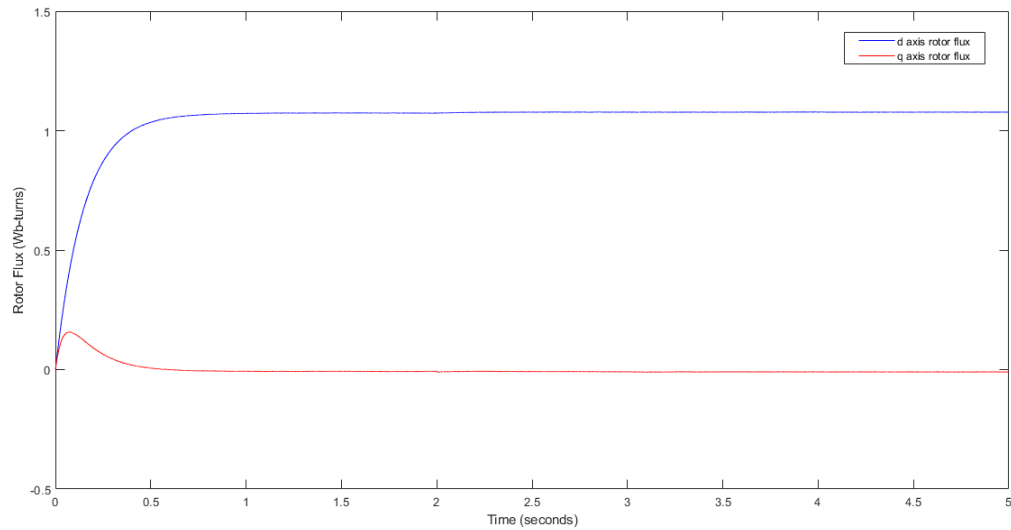


Figure 2.10: dq axes rotor flux plot for Indirect Vector control

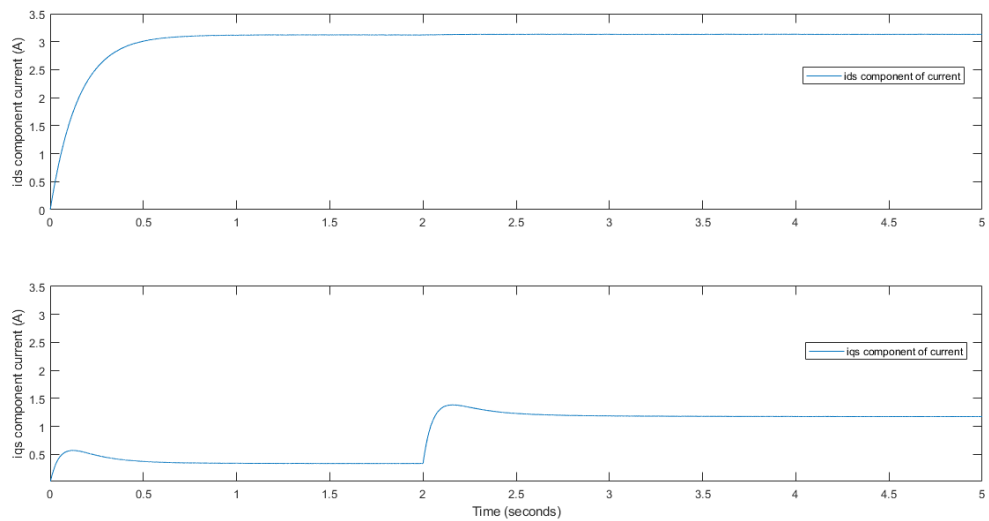


Figure 2.11: ids and iqs components of currents for Indirect Vector control

2.8 Conclusion

Rotor flux field-oriented vector control is preferred over stator flux FOC and Air gap FOC because of the inherent decoupling control of flux and torque and it is easy to implement. For accuracy and ease of implementation indirect vector control is chosen. The operations of CCVSI and VCVSI are discussed. To have desired switching frequency VCVSI is considered. The online rotor estimation method is used in the simulation of indirect vector control. Simulations have been carried out in MATLAB/Simulink and results show satisfactory response.

Chapter 3

Maximum Torque Per Ampere Control of Induction Motor

3.1 Introduction

Induction motors are typically manufactured to perform optimally at their rated loads. Unfortunately, the efficiency of induction motors drops dramatically when they are lightly loaded. In this chapter, we discuss Maximum Torque Per Ampere (MTPA) based rotor-flux-oriented vector control system that can be implemented to remedy the situation. Unlike the indirect vector control [18], the flux producing component in Maximum Torque per Ampere (MTPA) control method fluctuates in response to fluctuations in load. Therefore, the dynamic performance will be compromised. So it is attractive for things like electric cars (EVs) that do not require a quick dynamic reaction. The constant or slowly varying reference torque employed in EV applications allows for precise regulation of the reference flux in accordance with the MTPA control method requirement. Among the many documented methods of control aimed at improving the IM's operational efficiency is the MTPA control method [19]. This strategy ensures that the induction motor will draw the least amount of current from the stator possible under a given load.

3.2 Selection of the Flux Level for Maximum Torque Per Ampere Operation of an IM

Let us have a look at Indirect Vector control Equations again.

The expression of the torque as a function of the flux and torque producing components, i_{ds}^e and i_{qs}^e of the stator currents vector: from (2.40)

$$T_e = \frac{3}{2} \frac{P}{2} \frac{l_m^2}{l_r} i_{ds}^e i_{qs}^e$$

Writing (2.35)

$$\psi_{dr}^e = l_m i_{ds}^e$$

Substituting (2.35) into (2.40), we get

$$T_e = \frac{3}{2} \frac{P}{2} \frac{l_m}{l_r} \psi_{dr}^e i_{qs}^e \quad (3.1)$$

Writing (2.38)

$$\omega_{sl} = \frac{1}{\tau_r} \frac{i_{qs}^e}{i_{ds}^e}$$

Substitution of (2.35) in (2.38) by eliminating i_{ds}^e term.

$$\omega_{sl} = \frac{l_m}{\tau_r} \frac{i_{qs}^e}{\psi_{dr}^e} \quad (3.2)$$

Substitution of (3.2) into (3.1) and noting $\tau_r = \frac{l_r}{r_r}$ leads to the expression of the torque as a function of rotor flux magnitude ψ_{dr}^e and the slip frequency ω_{sl}

$$T_e = \frac{3}{2} \frac{P}{2} \frac{\psi_{dr}^{e^2}}{r_r} \omega_{sl} \quad (3.3)$$

if $|i_{dqs}|$ represent the magnitude value of the stator current vector and α is the angle between the stator current vector and rotor flux vector

$$i_{ds}^e = |i_{dqs}| \cos \alpha \quad (3.4)$$

$$i_{qs}^e = |i_{dqs}| \sin \alpha \quad (3.5)$$

Substitution (3.4) and (3.5) in (2.40) we get

$$T_e = \frac{3}{2} \frac{P}{2} \frac{l_m^2}{l_r} |i_{dqs}^e|^2 \sin \alpha \cos \alpha \quad (3.6)$$

$$T_e = \frac{3}{2} \frac{P}{2} \frac{l_m^2}{l_r} |i_{dqs}^e|^2 \frac{\sin 2\alpha}{2} \quad (3.7)$$

From (3.7) it is evident that maximum torque occurs when $\alpha=45^\circ$

then (3.4) and (3.5) becomes

$$i_{ds}^e = i_{ds}^e = \frac{|i_{dqs}^e|}{\sqrt{2}} = \frac{\psi_{dr}^e}{l_m} \quad (3.8)$$

Substitution (3.8) in (2.40) becomes

$$T_e = \frac{3}{2} \frac{P}{2} \frac{\psi_{dr}^{e,2}}{l_r} \quad (3.9)$$

Optimum rotor flux magnitude for the torque per ampere of stator current is maximum is

$$\psi_{dr}^e = \sqrt{\frac{4l_r T_e}{3P}} \quad (3.10)$$

corresponding slip frequency in electrical radians/seconds is given by

$$\omega_{sl} = \frac{r_r}{l_r} = \frac{1}{\tau_r} \quad (3.11)$$

Because of practical limitations, a constant minimal stator current cannot be guaranteed across the whole speed and torque ranges [20]. There are three limitations to the operation:

- Stator current is limited by the inverter current capability.
- Stator flux magnitude is limited to avoid saturation effect in that way torque is also limited.
- Stator voltage is limited by its rated value.

Based on (3.1), Figure 3.1a shows a plot between motor torque and torque component of current for various rotor flux. The torque versus slip frequency characteristics for different

constant rotor flux levels based on (3.3) is shown in Figure 3.1b superimposed on the conventional torque versus slip frequency characteristics shown at different constant stator current levels. Figure 3.1b shows that for any given stator current level, the torque can be maximized by choosing the appropriate rotor flux level. The selection of the rotor flux for MTPA operation depends on the stator current magnitude. The operating point is given by the intersection between the torque versus slip frequency characteristics at constant rotor flux and at constant stator current. The rotor flux selection for maximum torque operation and for a given current supply is shown in Figure 3.1c. However, for MTPA condition, i_{ds} should be equal to i_{qs} which is not possible for all working conditions due to operating constraints.

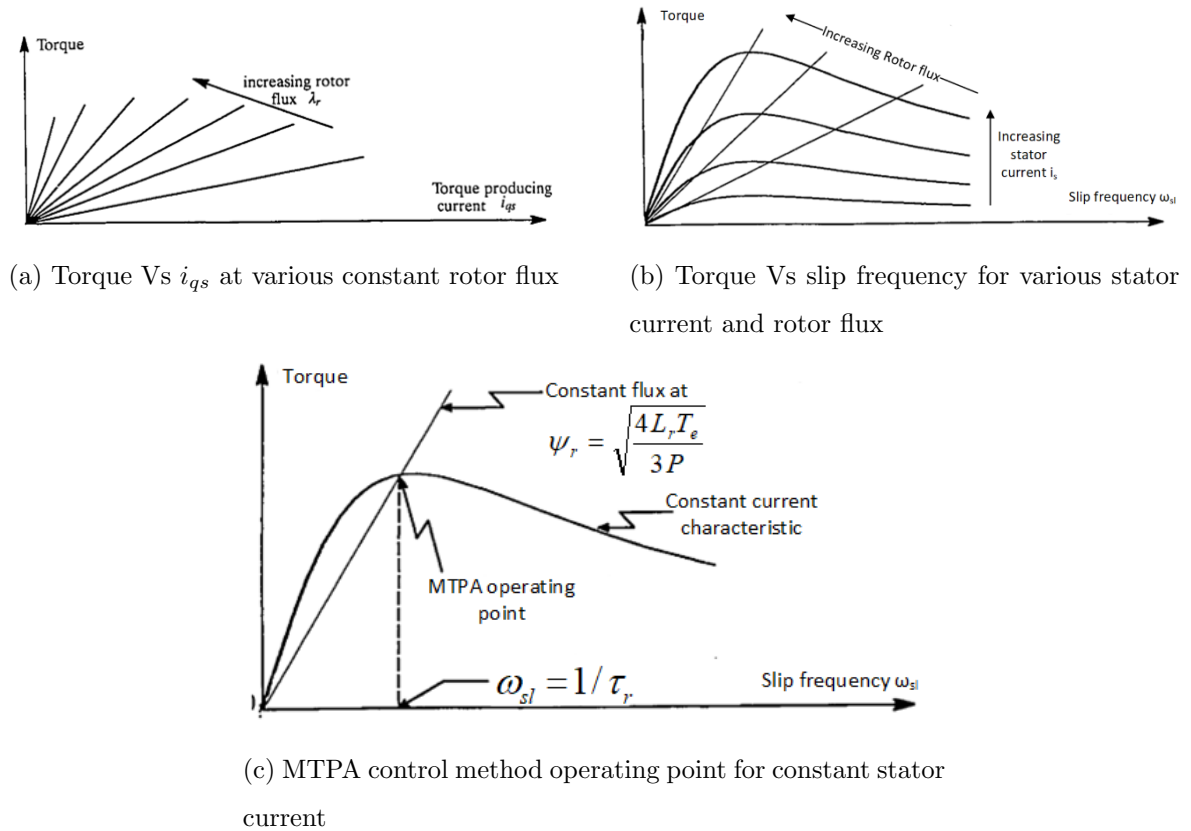


Figure 3.1: Rotor Flux Selection

3.3 MTPA Implementation

The block diagram in Figure 3.2 is similar to that of the rated rotor flux-oriented indirect vector control, with the exception of the reference current output. The reference currents are produced by the MTPA control method conditions described in the prior section. The outside loops are controlled by a single PI speed controller, while the inner loops are controlled by a pair of PI current controllers. Similar to the controllers employed in indirect vector control, these use a similar architecture. Gains for the controllers developed there can be used in this environment.

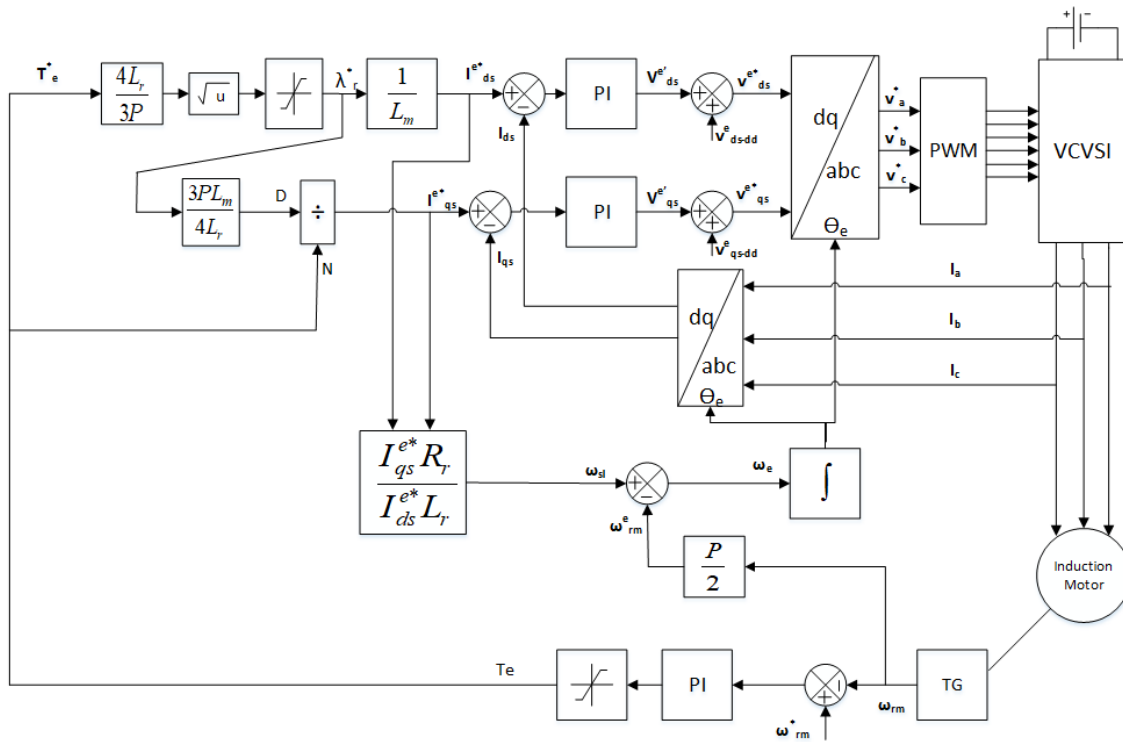


Figure 3.2: Block diagram implementation of MTPA control

3.4 Simulation Results

Figure 3.3 shows torque, speed, and phase currents. At $t=0$ sec, reference speed is 500 rpm and load torque is 1 N-m. Load torque of 3.5 N-m is given in a step change at $t=2$ sec with

reference speed = 1300 rpm. At low load, the phase currents of the MTPA control method are relatively small compared to the IV control method. Dynamic response is slow when compared to the IV control. Transient and steady-state response can be observed.

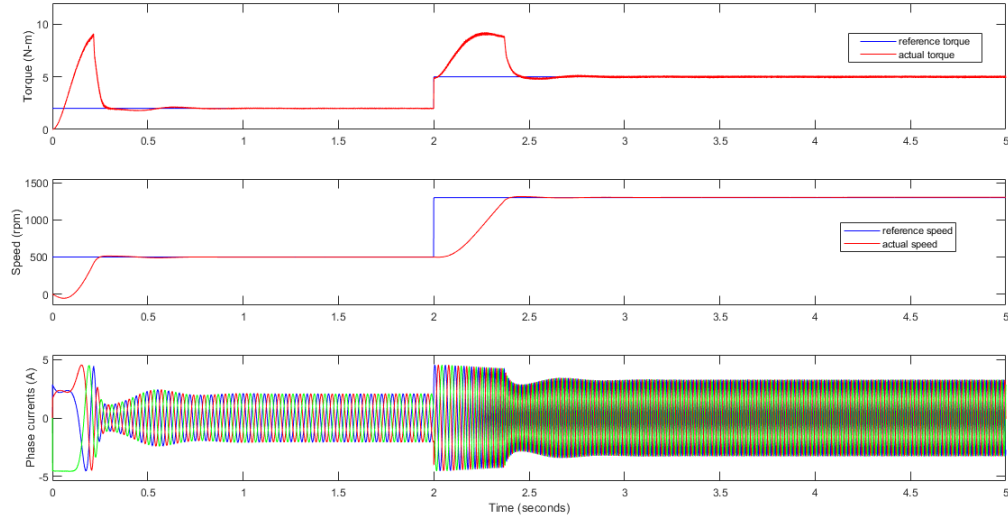


Figure 3.3: Torque, Speed, Phase currents plots are shown for MTPA control method

Figure 3.4 depicts rotor flux. According to the stator current, the optimal rotor flux will be estimated and applied so that maximum torque will occur to that stator current. Rotor flux will change according to the load condition. q-axis rotor flux is made zero in indirect vector control. Similarly in MTPA control also q-axis rotor flux is made zero.

Figure 3.5 represents i_{ds}^e , i_{qs}^e components of current. The major requirement of MTPA control is to keep the i_{ds}^e and i_{qs}^e components of the current equal

Figure 3.6 shows the comparison of the MTPA control method over the indirect vector control. In Figure 3.6 torque, phase currents, and rotor flux are shown in vertical order. At $t=0$ sec, torque = 1 N-m is given, and at $t=2$ sec step change of torque 2 N-m is given and finally at $t=4$ sec step change of torque 5 N-m is given. The whole observation is done at a constant speed of 1300 rpm. It can be seen that Stator phase currents are less in MTPA control when compared with indirect vector control when IM is at lightly loaded condition. In MTPA control, rotor flux is sensitive to the torque and gets modified to its optimal value so that minimum stator control will be drawn.

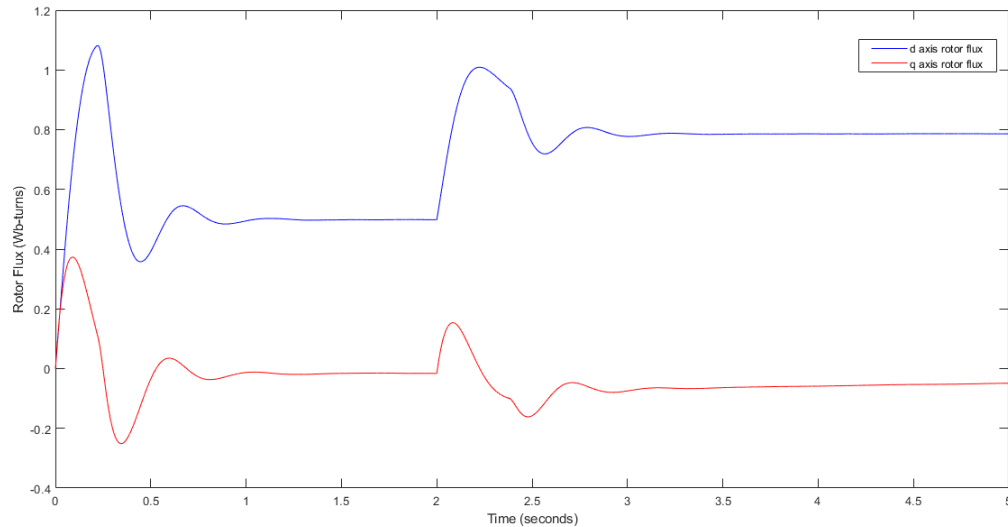


Figure 3.4: dq axes rotor flux plot for MTPA control method

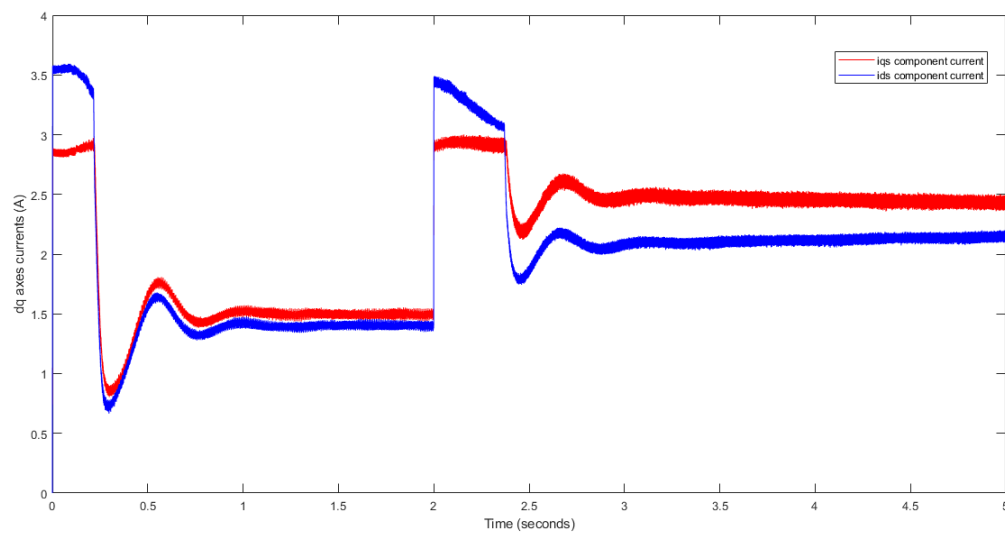


Figure 3.5: ids and iqs components of currents for MTPA control method

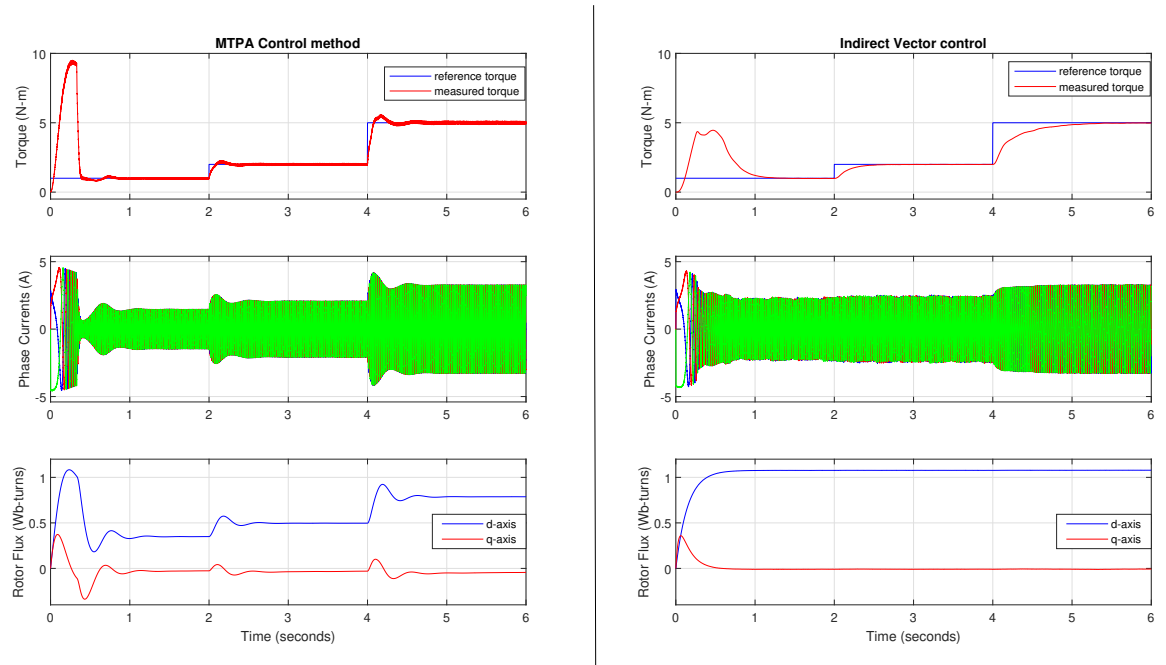


Figure 3.6: Torque, Phase currents, Rotor flux plots are shown for both MTPA control and Indirect Vector control methods

3.5 Conclusion

The principle of maximum torque per ampere control is discussed. The outcomes of the simulation are shown. Finally, the outcomes of indirect vector control simulations are compared to the results of MTPA control. The results show that MTPA control is more efficient than rotor oriented flux indirect vector control as minimal stator current will be drawn in the case of the former.

Chapter 4

Experimental Implementation and Results

4.1 Hardware Circuit

Three-phase supply is given to a $3 - \phi$ auto transformer which is then connected to a $3 - \phi$ rectifier. A DC link capacitor is used to get a more stable DC voltage across the $3 - \phi$ rectifier. The output of the $3 - \phi$ rectifier is connected to the $3 - \phi$ Inverter. The induction motor is supplied by the inverter. Mechanically coupled induction motor and DC generator set are used here. The DC generator connected to a resistive load which serves the purpose of loading the induction motor. A tacho generator is used for the speed measurement. The sensed speed is sent to the sensor board. Currents and voltages that are fed to the induction motor are passed through the voltage and current sensor board. With the help of an ADC protection card, sensed speed, currents, and voltages are sent to the DSP TMS320F28335. EPWM signals are generated according to the algorithm provided to the microcontroller. These EPWM signals are of low voltages, which is insufficient to feed the gate pulse of the inverter. So the signals are connected to Optocoupler Circuit which is used to increase the voltage levels, and isolation is also provided. An intelligent power module is used as the inverter. Figure 4.1 shows the schematic of the overall hardware. Figure 4.2 is the full view of the hardware setup. Figure 4.3 is the top view of the hardware setup.

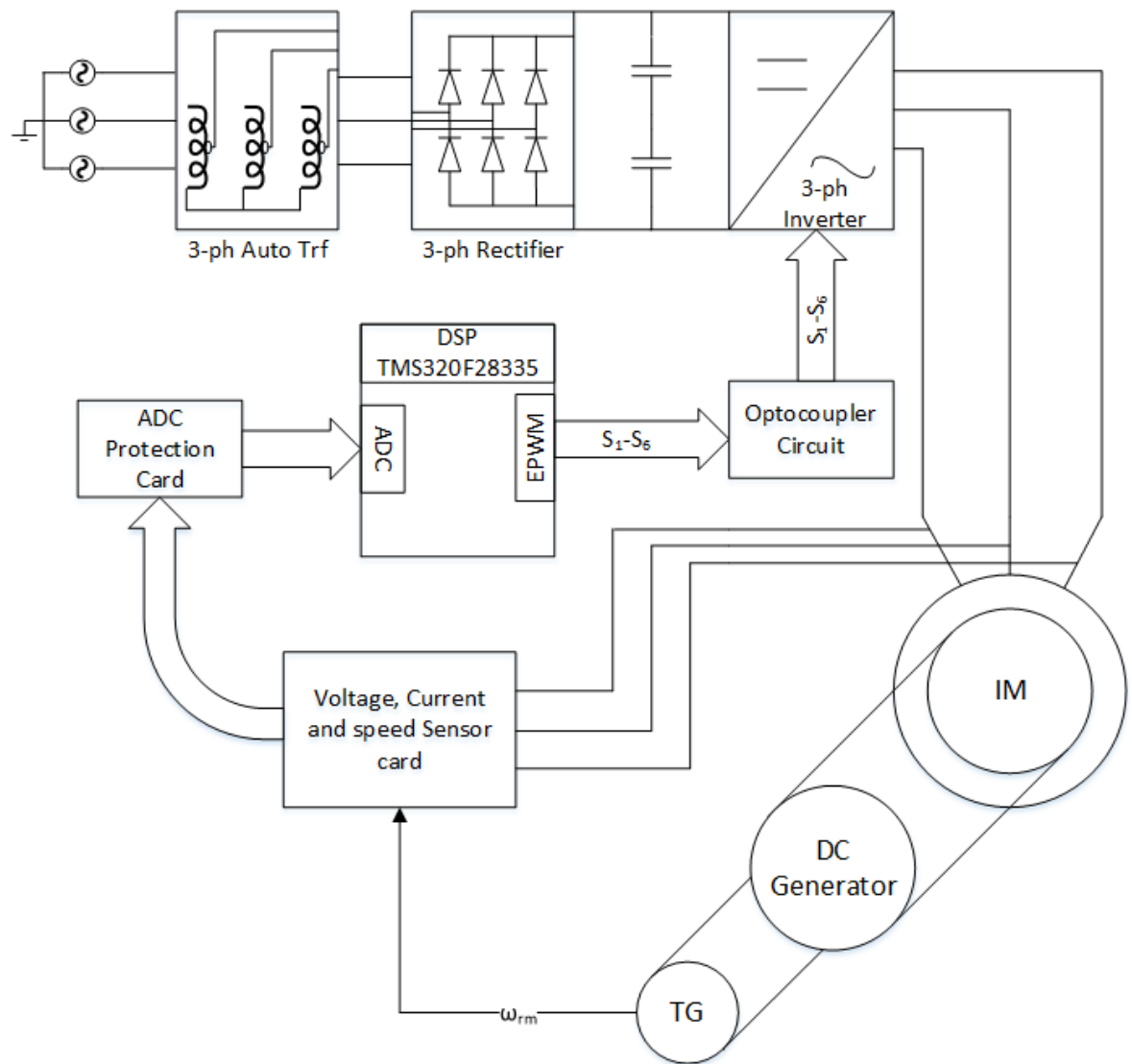


Figure 4.1: Overall hardware schematic



Figure 4.2: Full view of hardware setup

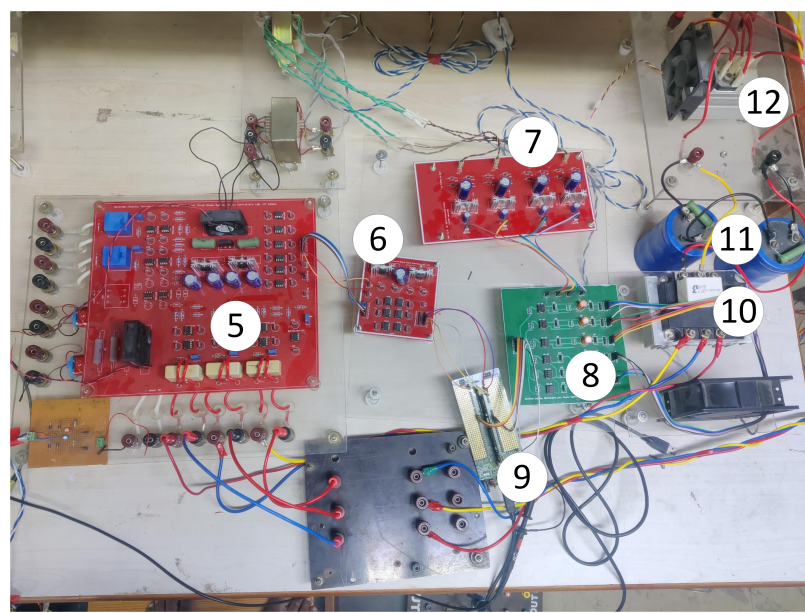


Figure 4.3: Top-view of hardware setup

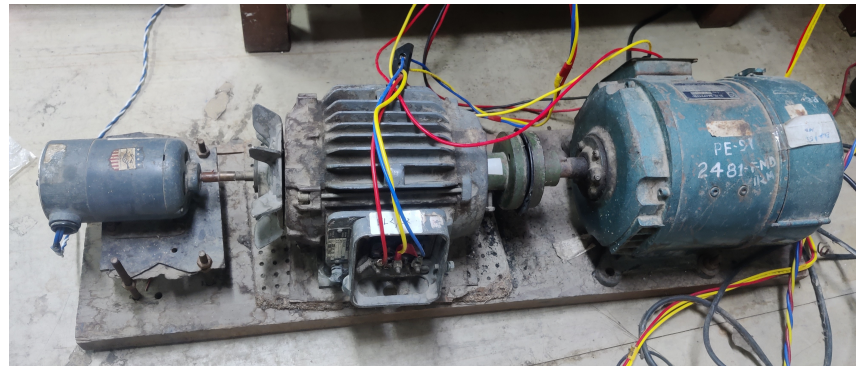


Figure 4.4: Motor-Generator-tachogenerator set

- | | | |
|----------------------------|---------------------------------|----------------------|
| 1)Motor-Generator set | 5)Voltage, current sensor board | 9)Microcontroller |
| 2)3 phase Auto transformer | 6)ADC protection card | 10)IPM module |
| 3)Resistive load | 7)Power Supply board | 11)DC link Capacitor |
| 4)field circuit for DC M/c | 8)Optocoupler | 12)3 phase rectifier |

4.2 Results

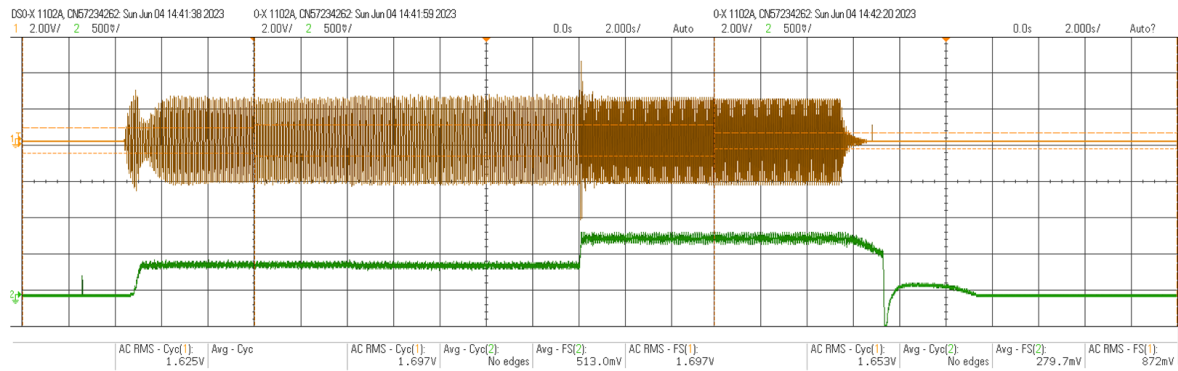


Figure 4.5: Indirect Vector control - a step change in speed from 350 rpm to 620 rpm at no-load. Ch1(brown): Phase current, Ch2(green): Speed

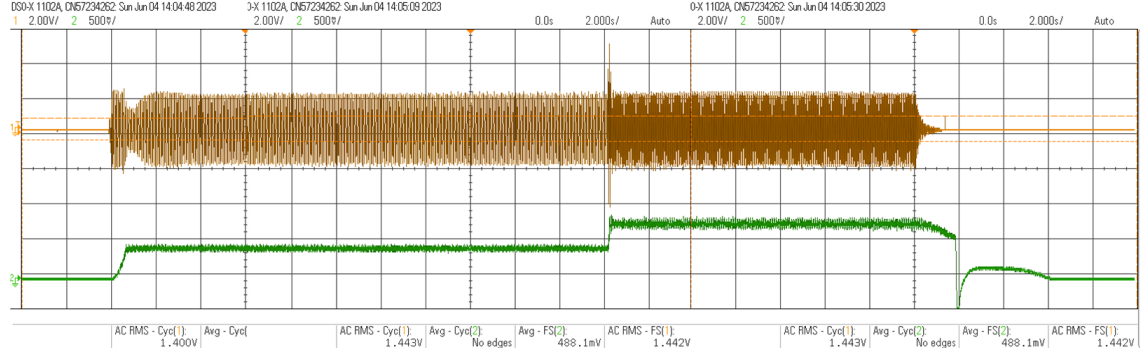
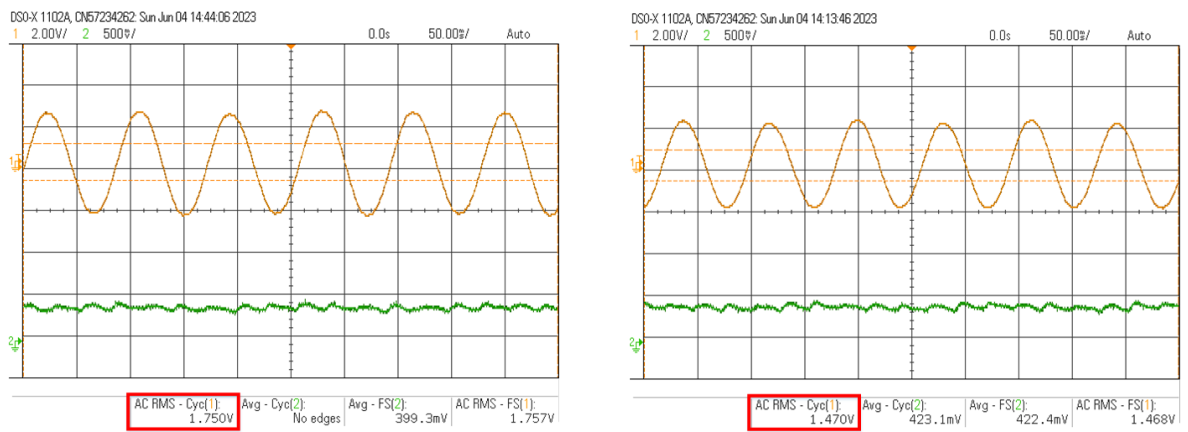


Figure 4.6: MTPA control - a step change in speed from 350 rpm to 620 rpm at no-load.
Ch1(brown): Phase current, Ch2(green): Speed

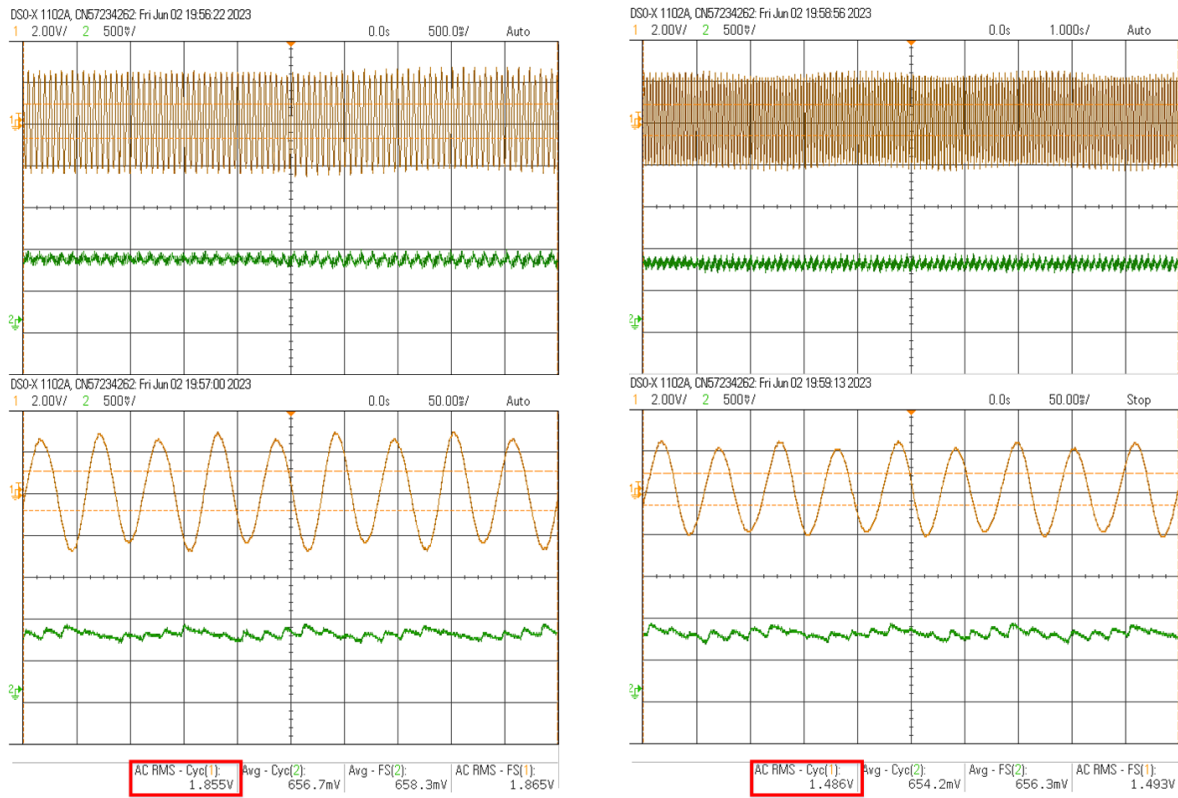


(a) IV control - zoomed portion at speed 350 rpm, Highlighted red box: phase current rms value **1.750 A**. Ch1(brown): Zoomed Phase current, Ch2(green): Speed

(b) MTPA control - zoomed portion at speed 350 rpm, Highlighted red box: phase current rms value **1.470 A**. Ch1(brown): Zoomed Phase current, Ch2(green): Speed

Figure 4.7: zoomed portion of Figures 4.5 and 4.6

To check IV control, a step change in speed from 350 to 620 rpm is given at no load. IV control phase current and speed waveforms are shown in Figure 4.5. Similarly to check MTPA control, a step change in speed from 350 to 620 rpm is given at no load. MTPA phase current and speed waveforms are shown in Figure 4.6. Zoomed view of IV and MTPA control methods are shown in Figure 4.7. We can notice that IV control draws 1.750 A whereas the MTPA method draws 1.470 A current. The DC machine is loaded with a resistive load. IV control in loaded condition draws 1.855 A (see Figure 4.8a) whereas MTPA in loaded condition draws 1.486 A (see Figure 4.8b). Current profile can be observed in zoomed view.



(a) IV (Loaded condition at 580 rpm) - Above screenshot is not zoomed. Below screenshot is zoomed portion, Highlighted red box: phase current rms value **1.855 A**. Ch1(brown): Zoomed Phase current, Ch2(green): Speed

(b) MTPA (Loaded condition at 580 rpm) - Above screenshot is not zoomed. Below screenshot is zoomed portion, Highlighted red box: phase current rms value **1.486 A**. Ch1(brown): Zoomed Phase current, Ch2(green): Speed

Figure 4.8: Loaded Condition (Two screenshots are merged together)

4.3 Conclusion

This chapter contains hardware setup and the experimental results. Both the indirect vector control and the MTPA control methods have been experimentally verified and the results are compared. MTPA control method draws lesser current for a given torque. Hence MTPA control of induction motor results in higher efficiency.

Chapter 5

Conclusion and Scope for Future Work

5.1 Conclusion

- Induction motor is modeled in the synchronous rotating reference frame using MATLAB/Simulink
- Indirect Rotor flux-oriented vector control is chosen over AFOC, SFOC methods. The voltage controlled voltage source inverter is designed and has been simulated in Simulink.
- Maximum torque per ampere (MTPA) control scheme is designed such that it provides maximum torque in the given stator current by varying rotor flux levels. It has been simulated and verified.
- Comparison of simulation results of IV control and MTPA control was shown. It has been evident MTPA control draws lesser current than IV control.
- For hardware DSP TMS320F28335 microcontroller is used for executing required algorithm for both the schemes.
- Indirect Vector control and MTPA control methods are implemented in hardware for no load (with step change in speed) and for loaded condition.

- Using tacho generator, current sensor, and voltage sensor are all parts of the experimental implementation. The ADC pins on the DSP should receive these signals. These pins have to be protected from high voltage where ADC protection card is used. DSP TMS320F28335 creates PWM signals. An optocoupler circuit has been designed to transfer microcontroller pulse width modulation signals to the inverter. This optocoupler circuit isolates low-power components from high-power components and provides gating signals to IGBT switches.

5.2 Scope for Future Work

- Since online rotor estimation is still a developing field of study, we have the opportunity to investigate new, more efficient methods.
- Speed sensor can be eliminated using speed sensorless control.
- Sinusoidal pulse width modulation (SPWM) technique is used for the VSI. However, it is possible to make better use of the DC link voltage by using space vector modulation (SVM).

References

- [1] D. W. Novotny and T. A. Lipo, *Vector control and dynamics of AC drives.* Wisconsin, USA, Oxford university press, 1996, vol. 41.
- [2] P. Vas, *Vector Control of AC Machine.* Oxford, U.K.: Clarendon, 1990.
- [3] E. Ho and P. Sen, “Decoupling control of induction motor drives,” *IEEE Transactions on Industrial Electronics*, vol. 35, no. 2, pp. 253–262, 1988.
- [4] N.Mohan, *Advanced Electric Drives: Analysis, Control and Modelling using Simulink.* Wiley, 2001.
- [5] R.Krishnan, *Electric Motor Drives : Modeling, Analysis, and Control.* Prentice Hall,Inc., Upper Saddle River, New Jersey c2001.
- [6] R. Marino, S. Peresada, and P. Tomei, “On-line rotor resistance estimation for induction motors,” in *Proceedings of IECON'94 - 20th Annual Conference of IEEE Industrial Electronics*, vol. 3, 1994, pp. 2137–2142 vol.3.
- [7] A. Ba-Razzouk, P. Sicard, and V. Rajagopalan, “A simple on-line method for rotor resistance updating in indirect rotor flux orientation,” in *IEEE 2002 28th Annual Conference of the Industrial Electronics Society. IECON 02*, vol. 1, 2002, pp. 317–322 vol.1.
- [8] A. Ebrahim and G. Murphy, “Adaptive backstepping control of a speed-sensorless induction motor under time-varying load torque and rotor resistance uncertainty,” in *2007 Thirty-Ninth Southeastern Symposium on System Theory*, 2007, pp. 341–346.

- [9] J. Moreira and T. Lipo, “A new method for rotor time constant tuning in indirect field oriented control,” in *21st Annual IEEE Conference on Power Electronics Specialists*, 1990, pp. 573–580.
- [10] M. Koyama, M. Yano, I. Kamiyama, and S. Yano, “Microprocessor-based vector control system for induction motor drives with rotor time constant identification function,” *IEEE Transactions on Industry Applications*, vol. IA-22, no. 3, pp. 453–459, 1986.
- [11] F.-J. Lin and H.-M. Su, “A high-performance induction motor drive with on-line rotor time-constant estimation,” *IEEE Transactions on Energy Conversion*, vol. 12, no. 4, pp. 297–303, 1997.
- [12] H. Toliyat, M. Arefeen, K. Rahman, and M. Ehsani, “Rotor time constant updating scheme for a rotor flux oriented induction motor drive,” in *Proceedings of PESC '95 - Power Electronics Specialist Conference*, vol. 2, 1995, pp. 1302–1306 vol.2.
- [13] J.-K. Seok and S.-K. Sul, “Induction motor parameter tuning for high performance drives,” in *Conference Record of 1998 IEEE Industry Applications Conference. Thirty-Third IAS Annual Meeting (Cat. No.98CH36242)*, vol. 1, 1998, pp. 633–639 vol.1.
- [14] H. M. Kojabadi, M. Abarzadeh, and L. Chang, “A comparative study of various methods of im’s rotor resistance estimation,” in *2015 IEEE Energy Conversion Congress and Exposition (ECCE)*, 2015, pp. 2884–2891.
- [15] K. L. V. Iyer, X. Lu, K. Mukherjee, and N. C. Kar, “Online stator and rotor resistance estimation scheme using swarm intelligence for induction motor drive in ev/hev,” in *2011 1st International Electric Drives Production Conference*, 2011, pp. 202–207.
- [16] G. Kenné, R. S. Simo, F. Lamnabhi-Lagarrigue, A. Arzandé, and J. C. Vannier, “An online simplified rotor resistance estimator for induction motors,” *IEEE Transactions on Control Systems Technology*, vol. 18, no. 5, pp. 1188–1194, 2010.
- [17] T. Matsuo and T. A. Lipo, ““a rotor parameter identification scheme for vector controlled induction motor drives,” in *IEEE Transactions Industry Applications*, vol. 24, Jan/Feb, 1998, pp. 151–159 vol.24.

- [18] F. M. Khater, R. Lorenz, D. Novotny, and K. Tang, “Selection of flux level in field-oriented induction machine controllers with consideration of magnetic saturation effects,” *IEEE Transactions on Industry Applications*, no. 2, pp. 276–282, 1987.
- [19] W. Sung, J. Shin, and Y.-s. Jeong, “Energy-efficient and robust control for high-performance induction motor drive with an application in electric vehicles,” *IEEE Transactions on Vehicular Technology*, vol. 61, no. 8, pp. 3394–3405, 2012.
- [20] P. Naganathan and S. Srinivas, “Maximum torque per ampere based direct torque control scheme of im drive for electrical vehicle applications,” in *2018 IEEE 18th International Power Electronics and Motion Control Conference (PEMC)*, 2018, pp. 256–261.

Appendix A

Motor Details

A.1 Name Plate Details

A.1.1 Induction Motor

Voltage - $415V_{ll-rms}$; Connection Type - Y; Current - 2.6A; Power - 1.5HP/1.1kW;
Speed - 1410 rpm; Frequency - 50Hz.

A.1.2 DC Generator

Power - 1 HP; Field Voltage - 230V; Output Voltage - 230V; Speed - 1500rpm;
Current - 4.5A.

A.2 Motor Parameters

Induction motor modeling requires all the motor parameters. So for finding the parameters below tests are conducted.

1. DC Test
2. No Load Test
3. Blocked Rotor Test
4. Retardation Test

A.3 DC Test

An induction motor per-phase stator resistance may be determined by applying an acceptable DC voltage across the two stator terminals and monitoring the resulting current.

$$R_{dc} = \frac{V_{dc}}{I_{dc}}$$

Also, we can measure dc resistance using a multimeter. Since the stator is star connected

$$R_{s,dc} = \frac{R_{dc}}{2}$$

$$R_{s,ac} = 1.25R_{s,dc} \quad \therefore \text{skin effect}$$

From the DC resistance test, $V_{dc} = 14.43V, I_{dc} = 1A$

$$R_{dc} = 14.43 \Omega;$$

$$R_{s,dc} = \frac{1.25 \times 14.43}{2} = 9.018 \Omega$$

Stator resistance per phase is $R_s = 9.018 \Omega$.

A.4 No-Load Test

In this experiment, rated voltage V_0 is applied. Motor is not loaded and corresponding current I_o and wattmeter readings are noted. Single wattmeter is used with the multiplication factor of 2.

Voltage(V_o)	Current(I_o)	$W_0(m = 2)$
418.3V	2.05A	25*2=50

Table A.1: No-Load table

A.5 Blocked Rotor Test

In this experiment, the rotor is blocked manually. Rated current I_{sc} is passed by increasing the supply voltage V_{sc} . Required Readings are noted. Single wattmeter is used with a multiplication factor of 1.

Voltage(V_{sc})	Current(I_{sc})	$W_{sc}(m = 1)$
98.5V	2.6A	81.25*1=81.25

Table A.2: Blocked Rotor table

A.6 Retardation Test

Retardation Test is used to determine the induction Motor-DC generator set's moment of inertia (J). The DC generator has been made into a DC motor for this experiment. Constant current is made to flow through the DC generator field winding. A three-phase rectifier is used to supply a DC to the armature terminals. The rated speed is reached by adjusting the voltage between the armature terminals. Each interval armature voltage and current are recorded, together with the associated speed (tacho-generator voltage), in [A.3](#). It is possible to determine the connection between power and speed from these measurements which is then plotted in matlab [A.2](#) (Plot-B). Now, we disconnect the armature's DC power source and use the DSO to record the speed vs time curve displayed in [A.1](#). From DSO, excel file is extracted and by using the moving average concept, Speed Vs time is plotted in matlab [A.2](#) (Plot-A).

Speed (rad/sec)	Speed (rpm)	V_{dc} (V)	I_{dc} (A)	$W_o = V_{dc}I_{dc} - I_{dc}^2R_a$ (W)	Tacho-generator output (V)
10.47	100	16.42	0.184	2.8499	0.051
21.25	203	32.4	0.19	5.98	0.2
31.31	299	46.2	0.20	9.03	0.324
42.51	406	62	0.21	12.79	0.493
62.83	600	90.4	0.223	19.90	0.793
73.32	700.2	105	0.226	23.47	0.877
83.93	801.5	120.5	0.231	27.56	1.042
94.45	902	135	0.235	31.44	1.155
104.82	1001	150	0.242	36	1.295
115.714	1105	165	0.247	40.44	1.449
126.186	1205	179.5	0.256	45.620	1.567
136.344	1302	194	0.259	49.90	1.688
147.130	1405	209	0.265	55.02	1.834
157.183	1501	223	0.275	60.94	1.970

Table A.3: Retardation Test

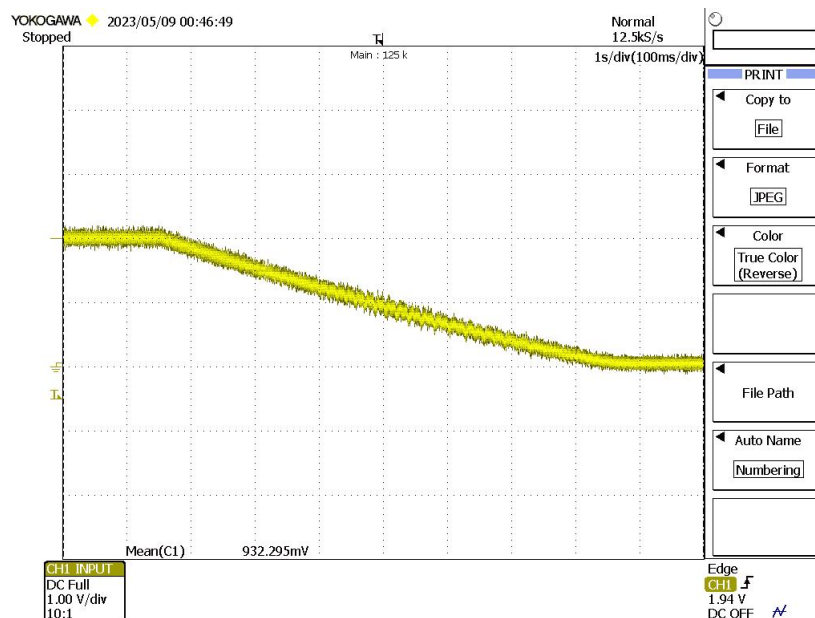


Figure A.1: Speed Vs time plot

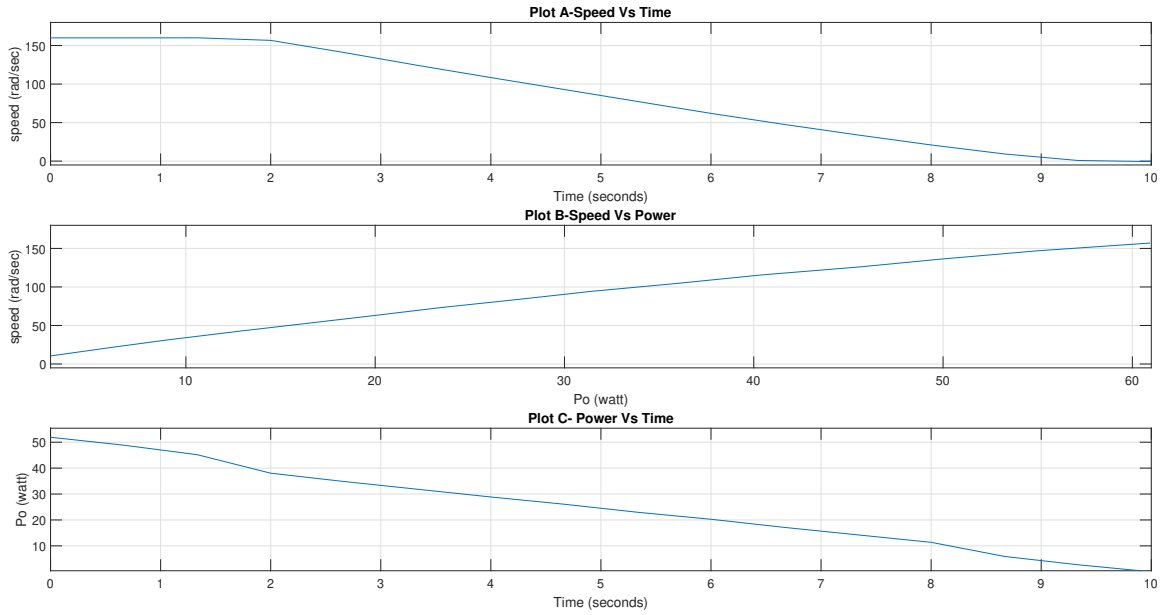


Figure A.2: Plot A - Speed Vs Time; Plot B - Speed Vs Power; Plot C - Power Vs Time

Using [A.2](#) (Plot-A) and [A.2](#) (Plot-B), Power Vs Time is plotted in Matlab which is shown in [A.2](#) (Plot-C).

The moment of Inertia(J) can be calculated using the area under the Power Vs time plot. From Figure [A.2](#)(Plot-C) the area under the Power Vs time plot is calculated as 198.43 Joules.

$$\frac{1}{2} \times J \times \omega_{ro}^2 = 198.43 \quad (\text{A.1})$$

where $\omega_{ro}=157.66$ rad/sec is rotor shaft speed

$$J = \frac{198.43 \times 2}{157.66^2} = 0.01596 \text{ Kgm}^2$$

$$\therefore J = 0.01596 \text{ Kgm}^2$$

The friction coefficient (B) is neglected.

A.7 Calculations for Induction Motor Parameters

From the above tests conducted, we can find per phase equivalent circuit parameters of IM.

Using No-Load experiment,

$$\begin{aligned}
V_o &= \frac{418.3}{\sqrt{3}} V; I_0 &= 2.05 A; P_o &= 50 W \\
Z_o &= \frac{V_o}{I_o} = \frac{\left(\frac{418.3}{\sqrt{3}}\right)}{2.05} = 117.81 \Omega; \\
R_o &= \frac{P_o}{I_o^2} = \frac{50}{2.05^2} = 11.897 \Omega; \\
X_o &= \sqrt{Z_o^2 - R_o^2} = 117.206 \Omega;
\end{aligned}$$

Using Blocked Rotor experiment,

$$\begin{aligned}
V_{sc} &= \frac{98.5}{\sqrt{3}} V; I_{sc} &= 2.6 A; P_{sc} &= 81.25 W \\
Z_{sc} &= \frac{V_{sc}}{I_{sc}} = \frac{\left(\frac{98.5}{\sqrt{3}}\right)}{2.6} = 21.873 \Omega; \\
R_{sc} &= \frac{P_{sc}}{I_{sc}^2} = \frac{81.25}{2.6^2} = 12.019 \Omega; \\
X_{sc} &= \sqrt{Z_{sc}^2 - R_{sc}^2} = 18.274 \Omega;
\end{aligned}$$

Leakage reactance is defined as follows by NEMA Design A:

$$\begin{aligned}
X_s &= X_r = \frac{X_{sc}}{2} = 9.137 \Omega; \\
X_m &= X_o - X_s = 117.206 - 9.137 = 108.069 \Omega; \\
R_r &= (R_{sc} - R_s) = 12.019 - 9.018 = 3.001 \Omega;
\end{aligned}$$

Mutual inductance $L_m = 0.344$ H,

Stator and Rotor Leakage inductances $L_{ls} = L_{lr} = 0.029$ H.

Therefore all the motor parameters are,

Parameter	Value	Parameter	Value
R_s	9.018 Ω	L_{lr}	0.029H
R_r	3.001 Ω	L_s	0.373H
L_m	0.344H	L_r	0.373H
L_{ls}	0.029H	J	0.01596 Kgm ²

Table A.4: Induction Motor Parameters

Appendix B

Hardware Specifications

B.1 Intelligent Power Module (IPM)

Mitsubishi intelligent power module PM50RVA120 is used as a voltage source inverter.



Figure B.1: Mitsubishi Intelligent Power Module

Specifications

- Voltage : 1200 V AC
- Current : 50 A
- Switching frequency : 20 kHz (Max)
- Switches Type : IGBT.

B.2 Voltage Sensor

The LV25-P transducer is used for Voltage measurement.

Specifications

- Primary nominal rms current : 10 mA.
- Voltage : 10-500 V
- Conversion ratio : 2500 : 1000
- Supply Voltage : ± 12 - ± 15 V

B.3 Current Sensor

The LA55-P current transducer is used to measure electrical current.

Specifications

- Primary nominal rms current : 50 A.
- Conversion ratio : 1 : 1000
- Supply Voltage : ± 12 - ± 15 V

B.4 Speed Sensor Board

The tacho generator's output voltage reflects the motor speed.

Name Plate Details :

- Volts/ rpm : 19.9 V/1000 rpm
- Polarity : AC
- Maximum speed : 5000 rpm

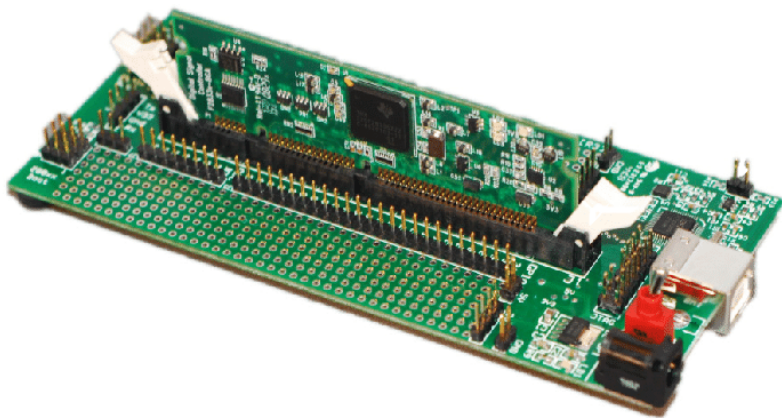


Figure B.2: TMS320F28335 Experimental Kit

B.5 DSP Kit

Texas Instrument's TMS320F28335 Digital Signal controller has been used for the hardware implementation of the desired algorithm.

Specification

- Maximum Operating frequency : 150 MHz
- 12-bit ADC : 16 channels
- Programmable GPIOs : 88 pins
- PWM outputs : 18 pins
- Watch dog timer